A 1600 year-long sedimentary record of tsunamis and hurricanes in the Lesser Antilles (Scrub Island, Anguilla)

M Biguenet, Pierre Sabatier, E Chaumillon, C Chagué, Fabien Arnaud, F Jorissen, T Coulombier, E Geba, L Cordrie, P Vacher, et al.

1600 year-long sedimentary record of tsunamis and hurricanes in the Lesser Antilles (Scrub Island, Anguilla)

Biguenet, M.[a,b], Sabatier, P.[b], Chaumillon, E.[a], Chagué, C.[c], Arnaud, F.[b], Jorissen, F.[d], Coulombier, T.[a], Geba, E.[a], Cordrie, L.[e,f], Vacher, P.[g], Develle, A.L.[b], Chalmin, E.[b], Soufi, F.[b], Feuillet, N.[e]

[a] Université de la Rochelle, UMR 7266 LIENSs, Bâtiment Marie Curie, avenue Michel Crépeau, 17042 La Rochelle cedex, France.

[b] Université Savoie Mont Blanc, UMR 5204 EDYTEM, Bâtiment « Pôle Montagne », 5 bd de la mer Caspienne, 73376 Le Bourget du Lac cedex, France.

[c] UNSW Sydney, Sydney 2252, NSW, Australia.

[d] Université de Angers, UMR CNRS 6112 LPG, 2 boulevard Lavoisier, 49045 Angers Cedex 1, France.

[e] Institut de Physique du Globe de Paris, Université de Paris, CNRS, 75005 Paris, France.

[f] CEA, DAM, DIF, F-91297 Arpajon, France.

[g] Laboratoire SYMME, domaine Universitaire BP 80439, 74944 Annecy le Vieux Cedex, France.

Abstract

The Lesser Antilles are a densely populated and a very touristic region exposed to many short-term hazards such as hurricanes and tsunamis. However, the historical catalog of these events is too short to allow risk assessment and return period estimations, and it needs to be completed with long-term geological records. Two sediment cores were sampled in March 2018 in a small coastal lagoon on Scrub Island (north eastern Caribbean). Here, we present sedimentological, geochemical, microfaunal and chronological analyses that enabled us to identify 25 sandy layers resulting from high energy marine floods. Two of these layers were interpreted as tsunami deposits based on sedimentological and geochemical evidence. The most recent deposit is associated with the transatlantic tsunami triggered by the 1755 AD Lisbon earthquake. The older is the thickest sandy layer recorded in the lagoon and is dated at 1415 cal. AD (1364-1469 cal. AD). This event was recorded in both the northern and the southern part of the Caribbean, with its large extent supporting a tsunamigenic origin. The 23 remaining sandy

layers were interpreted as resulting from hurricanes, with the three most recent layers being associated with historical hurricanes. This new 1600 year-long reconstructed chronicle, has been compared to other published hurricane chronicles from the region. Scrub chronicle is the most eastern site and displays similarities with that of the Bahamas, while it is in antiphase with that of the north eastern US coast. This regional comparison may provide evidence of a latitudinal forcing for the hurricane tracks through time in relation to climate fluctuations.

Keywords: Coastal hazards; tsunamis; hurricanes; Lesser Antilles; lagoons sediment; late Holocene

1. Introduction

Worldwide, an increasing number of people living along the coasts are threatened by natural hazards (earthquakes, volcanoes, hurricanes, tsunamis and marine floods). To better constrain the risk due to natural hazards in a region, it is crucial to determine the recurrence interval and the intensity of a given hazard. Historical records of these events are of prime importance to this goal but they are often too short. Thus, a geological record establishing time-series extending back thousands of years is the only way to address the long-term recurrence of natural hazards (i.e. Atwater, 1987; Nanayama et al., 2003; Scileppi and Donnelly, 2007; Jankaew et al., 2008; Woodruff et al., 2009). Large overwash related to hurricanes and tsunamis that can occur in a few hours may strongly affect the coastal landscape and ecosystems for millennia.

Large tsunami waves may transport large fragments of rocks or coral ripped off the coasts and reefs over several kilometers, at elevation of several meters (Goto et al., 2013; Atwater et al., 2017), they can breach the coastal dunes (e.g. Atwater et al., 2012), modify the geography and ecosystems of coastal lakes and pond by flooding them with tons of coarse-grained sand, salt marine water, and fauna (Chagué-Goff, 2010; Scheucher and Vortisch, 2011; Chagué-Goff et al., 2017). The sediment archives in such environment record the traces of past overwash and can be used to reconstruct the intensity and recurrence of these event (e.g., Atwater, 1987; Liu and Fearn, 1993, 2000; Donnelly et al., 2001; Nanayama et al., 2003; Scileppi and Donnelly, 2007; Sabatier et al., 2008; Woodruff et al., 2009;

Chaumillon et al., 2017). It is however still very difficult to distinguish storm and tsunami deposits and this remain a main obstacle against progression in knowledge on hazard related two high energy events in region where they can both occur.

Engel et al. (2016) have already summarized the known criteria to identify tsunami deposits in the Caribbean. Among the most cited arguments, there are: internal mud laminae, intraclasts (rip up clast), truncated flame structures, or backflow induced structures. Storm deposits will tend to have many parallel, cross laminations and climbing ripples (Morton et al., 2007b; Baumann, 2017). Moreover, storm deposits will generally tend to be more restricted across the shore than tsunami deposits because of the storm shorter wavelengths (Morton et al., 2007). Added to the sedimentological and morphological criteria, others proxies of a marine source such as geochemical (e.g. Chagué-Goff, 2010; Chagué-Goff et al., 2017; Riou et al., 2019) and microfaunal (e.g. Engel et al., 2013) markers may also help to characterize tsunami deposits. Most studies have focused on either hurricane or tsunami deposits but rarely on both within the same environment (e.g., Nanayama et al., 2000; Goff et al., 2004).

Here, we investigate the sedimentary record preserved in a coastal lagoon on a small Caribbean Island of the Lesser Antilles arc (Scrub, Anguilla). Hurricanes represent a major hazard in the Lesser Antilles arc because they occur frequently (Oliva et al., 2018), with recent very destructive events such as Hurricane Irma (2017 AD, Cangialosi, et al., 2018), Donna (1960 AD; Dunn, 1961) or Luis (1995 AD; Hoggarth, 2001). Furthermore, the densely populated and highly touristic islands of the Lesser Antilles arc are threatened by large earthquakes (Feuillet et al., 2011), volcanic eruptions (Boudon et al., 2007) and tsunamis (Engel et al., 2016). However, these natural hazards are still poorly constrained mainly because the historical record is too short.

This new sedimentary archive constitutes a unique opportunity to investigate the impact of both hurricanes and tsunamis on coastal lagoons, better understand the sedimentary record of past events on a multi-decadal to centennial timescale and find clues to decipher between past hurricane and tsunami events along the coasts.

We applied a multiproxy approach with sedimentological, geochemical and microfaunal analyses as well as radiocarbon and short-lived radionuclides dating of two one-meter-long sediment cores. We reveal the existence of many sand layers interbedded within the lagoon autochthonous sedimentation.

By combining our results with other data available in the literature, we discuss the origin of these sand layers to further establish a chronology for tsunami and hurricane events. We then discussed criteria to distinguish between tsunami and hurricane deposits in this record. On the basis of our catalog of hurricane events we discuss on the modulation of hurricane activity by climate forcing.

2. Study area

In the following section the geomorphology, geology and geodynamic characteristics of the study area are described, as well as the main known high energy events from historical data and sedimentary records.

2.1. Geomorphologic and geologic settings

The Lesser Antilles form a 850 km-long island arc in the Caribbean Sea (Fig. 1A) (Scheffers et al., 2005). Scrub Island is located in the northern part of the Lesser Antilles arc, southeast of the Anegada Passage. It belongs to a group of islands (including Saint-Martin, Saint-Barthelemy, Anguilla) surrounded by a large 40 m-deep carbonate platform called the Anguilla-Saint-Barthelemy platform (Fig. 1B). Scrub Island and many other small neighboring islets are inhabited. Scrub Island is 3.5 km-long from east to west and about 1.5 km-wide from north to south (Fig. 1C). It consists of low relief limestones, with the highest point about 25 m above sea level (a.s.l.) close to the center of the island (Fig. 1C). The island displays a karstic limestone landscape, which transfers the rainfall directly into the fractured basement, before it flows into the sea (Bruce, 2000). Therefore, the vegetation, mostly small bushes and cactus species, is sparse. Permanent water bodies are limited on Scrub Island and include three shallow ponds that could have been isolated from the open ocean after the last higher sea level stand, as suggested for the Anguilla ponds (Bruce, 2000). In this study, we focus on the westernmost lagoon, separated from the ocean by a 2 to 5 m-high and 50 m-wide sandy barrier covered by small bushes at the top (Fig. 1D). This salty lagoon is approximately 400 m-long and 130 m-wide and very shallow, with a maximum water depth of 80 cm (as observed in March 2018). Examination of Google

Earth aerial photographs from 2003 to 2020 suggests that no barrier breach has occurred over the last 17 years.

2.2. Past tsunamis in the Lesser Antilles

The Lesser Antilles arc results from the subduction of the American plate under the Caribbean plate at 2 cm yr^{-1} (DeMets et al., 2000), with numerous volcanoes and active faults that can generate tsunamis. Several tsunamis have been reported during the historical period in the Lesser Antilles arc (Zahibo and Pelinovsky, 2001; Lander et al., 2002; Engel et al., 2016), with their origin including local or more distant earthquakes (Reid and Taber, 1920; Pelinovsky et al., 2004; Zahibo et al., 2005; Roger et al., 2011; Harbitz et al., 2012; Cordrie et al., 2019), volcanic processes (e.g., Pelinovsky et al., 2004; Watt et al., 2012), or transoceanic and associated to far-field sources (Roger et al., 2011).

The oldest historical tsunami observed in the Lesser Antilles occurred on 6 April 1690 AD in Antigua, Saint Kitts and Nevis. This event was triggered by an earthquake with a magnitude estimated at Ms 8 (Dorel, 1981).

The most important reported tsunami occurred in 1755 AD. This event is related to the major earthquake (Mw=8-9 class earthquake) that destroyed Lisbon (Portugal) on 1 November 1755 (Chester, 2001), and generated a transoceanic tsunami that hit the coasts of Spain, Portugal, Morocco but also the Caribbean (Roger et al., 2011). The tsunami was observed at 17 locations across the north-eastern Caribbean from Dominica to Hispaniola, with a maximum wave height of 6.4 m at Saba Island (Fig. 1A) (Fuentes et al., 2017).

On 30 November 1823 AD, the Saint Pierre harbour in Martinique was hit by a strong earthquake (epicenter coordinates: 14.4° N 61.1° W; NOAA/NESDIS data) which was followed by a tsunami 25 minutes later (Lander et al., 2002).

On 8 February 1843 AD a M8-class earthquake occurred between Antigua and Guadeloupe (e.g., Sainte-Claire Deville, 1843; Bernard and Lambert, 1988; Nathalie Feuillet et al., 2011; Hough, 2013). Despite

its magnitude, this event may have triggered only a small tsunami which was observed only in English harbour at Antigua (with a wave amplitude of 1.2 m) and Nevis (Shepherd, 1992).

Another historical tsunami occurred in the British Virgin Islands on 18 November 1867 AD (Reid and Taber, 1920). The wave reached 4 to 6-m height according to the observations and exceeded 10m at Guadeloupe, which is the highest reported value of tsunami height in the Caribbean Sea (Lander et al., 2002). The tsunami followed a strong earthquake felt in all the British Virgin Islands, but the origin of the event remains poorly constrained (Reid and Taber, 1920; Zahibo et al., 2003).

More recently, a tsunami was generated in 2004 by the M 6.3 normal fault earthquake of Les Saintes in the Guadeloupe archipelago (Le Friant et al., 2008; N. Feuillet et al., 2011; Cordrie et al., 2019). This earthquake generated small waves with 2 m of run-up in several bays of Les Saintes, a group of islands in the South of Guadeloupe (Cordrie et al., 2019).

Other historical tsunamis triggered by volcanic eruptions are reported in this region, such as the Montserrat in 2002 (Pelinovsky et al., 2004) but these events are beyond the scope of this study as there are more local and may not hit Scrub Island.

North of the Lesser Antilles arc, beyond the Anegada passage, evidences of extreme overwash have been found in sedimentary records along the coasts and in hypersaline lagoon of Anegada (British Virgin Islands, Atwater et al., 2012, 2017). ^{14}C dating of coral boulders, shells and organic remains indicates that these overwash occurred in the Middle age (between 1200 and 1480 cal. AD). This event has been attributed to an extraordinary storm or a tsunami of nearby origin (rupture of the Puerto-Rico megathrust, outer-rise normal faulting). In St Thomas (US Virgin Islands), four coastal ponds and a mangrove site contain a record of a tsunami also dated with radiocarbon from plant remains between 1200 and 1450 cal. AD (Fuentes et al., 2017).

2.3. Past hurricanes in the Lesser Antilles

Numerous hurricanes have been reported in the Lesser Antilles Arc. They occur mostly between July and November with frequency, magnitude and trajectory changes from one year to another (Garnier et al., 2015). They are influenced by large regional climate oscillations such as the El Niño Southern Oscillation (ENSO) (Jury et al., 2007), the Atlantic Multidecadal Oscillation (AMO) (Burn et al., 2016) or the ITCZ (Van Hengstum et al., 2016), with the latter authors suggesting that the ITCZ position modulates the hurricane activity in the Caribbean. It has been argued that when the ITCZ migrates further north, the vertical shear winds decrease in the Atlantic Hurricane Development Zone, facilitating the formation of intense hurricanes. Furthermore, the ITCZ position may also modulate the hurricane tracks through time. Baldini et al. (2016) propose that during cooling periods, the ITCZ southward displacement enables an east-west hurricane track in the south Caribbean. In contrast, during a warming period, the ITCZ moves northward, which would then shift the hurricane track to the northeast of the Caribbean, close to Scrub Island and the Bahamas.

Sedimentary studies along the coasts of various islands and in lagoons have revealed deposits related to past hurricanes (Donnelly and Woodruff, 2007; McCloskey and Keller, 2009; Malaizé et al., 2011; Donnelly et al., 2015; Denommee et al., 2015; Wallace et al., 2019), but no paleotempestology studies have been conducted in Anguilla or Scrub Island.

The current observational record in the Lesser Antilles began around 1850 AD and the National Oceanic and Atmospheric Administration (NOAA) documented 13 hurricanes that passed within 30 km of the island of Scrub from 1852 to 2017 (coast.noaa.gov/hurricanes, 2020; Table 1).

This region was struck by the extremely strong category 5 Hurricane Irma in September 2017 (Table 1, Fig. 2). This event is unprecedented in the historical record (Cangialosi, et al., 2018). It resulted in major damage, destroying many towns and killing 47 people before continuing its route north-westwards, where it impacted the Virgin Islands and Florida (Cangialosi et al., 2018). Other category 3 hurricanes, such as Donna (1960 AD (Dunn, 1961) and Dog (1950 AD) (coast.noaa.gov/hurricanes, 2020) with

187 south-west trajectories relative to Scrub Island (Fig. 2), strongly affected this part of the Lesser Antilles
188 (Table 1).
189

190 3. Material and methods

191 3.1. Sampling and core description

192 Fieldwork took place in March 2018, with the aim of recovering a sedimentary record deposited
193 in Scrub Island westernmost lagoon. Two one-meter-long sediment cores were sampled at 80 cm water
194 depth using an Uwitec gravity corer with a hammer. The location of cores was chosen along a transect
195 perpendicular to the coast. SCR1-18-01 was taken just behind the dune whereas SCR1-18-03 was taken
196 at the opposite side of the lagoon (150 m east of core SCR1-18-01), in distal position relative to potential
197 washovers. The cores were horizontally stored in a walk-in cooler in the laboratory, before being split,
198 photographed, described in detail and subsampled.
199

200 3.2. Sedimentological and mineralogical analyses

201 Grain-size analyses were carried out at the EDYTEM laboratory using a Beckman Coulter LS
202 13 320 XR particle size analyser using sonication, with a range size between 0.010 µm and 3000 µm.
203 The sampling step was about 5 mm through core SCR1-18-01 respecting facies boundaries. The mean
204 grain size curve and the grain size contour plot were produced using the Matlab software.
205 Core SCR1-18-01 was scanned at the SYMME laboratory (Annecy, France) using an X-ray
206 tomography system (Easytom XL 150 from RX SOLUTION society) at 150 kV and 200 µA. The core
207 was cut in two sections (110 to 70 cm and 70 to 0 cm), which were scanned one after the other. The
208 acquisition time was about 1 hour per core (for each section, 7 successive scans by translating along the
209 beam were necessary to cover the entire volume of the core). The reconstructed data are sets of 16 bits
210 Tiff image files representing cross-sections of the cores (horizontal slices from top to base). The image
211 resolution (voxel size) is 55 µm for the lower 40 cm and 85 µm for the upper 70 cm of the core. The
212 total number of images available for the core is 12,992 (6,048 + 6,944). For each section, the vertical

cross-sections were reconstructed using the Image J software and including the Fiji distribution extension (Schindelin et al., 2012).

X-ray diffraction (XRD) analyses were performed on core SCR1-18-01 with a sampling step of 5 cm to identify the mineralogical species. The diffraction was performed on powder in reflection mode on sample holder of the ASTRE platform of the Université Savoie Mont-Blanc (XRD: INEL; tube CoKα=0,1789 nm X-ray; slit of 1.5 x 0.1; reflection mode; generator INEL XRG3D 30 mA, 30kV; sensitive detector of curve position INEL CPS120 at 0,29° in resolution at FWHM). The mineralogical species were identified using the Match! software. The first 10 cm of the core were not analyzed for mineralogy as they were required for the measurements of short-lived radionuclides (^{210}Pb, ^{137}Cs and ^{241}Am).

3.3. Geochemical analyses

X-ray fluorescence (XRF) analyses were carried out on both cores at the EDYTEM laboratory using the Avaatech Core Scanner (Avaatech XRF Technology, Alkmaar, The Netherlands) with a rhodium anode and choosing a 1 mm step resolution (Richter et al., 2006). Two runs were used to detect light and heavy weight elements: a run at 10 kV, 0.2 mA for 20 s and a run at 30kV, 0.3 mA for 20 s. A Principal Component Analysis (PCA) was performed on the XRF core scanner data for core SCR1-18-01 using the open-source software R (R Core Team, 2014) to highlight chemical endmembers (e.g., Sabatier et al., 2010) and element correlations.

Loss on ignition (LOI) analyses were performed on core SCR1-18-01 with a sample step of 5 cm to quantify the amount of organic matter (LOI550) and carbonates (LOI950) in the different sedimentary units, according to the protocol described by Heiri et al. (2001). It was noted that for this type of sediment (carbonate-rich), the four hours at 950°C of the protocol were not sufficient to burn all carbonates. Thus, the percentages of carbonates presented are about 20% lower than its real content. After different heating timing, the relevant percentage of carbonates was reached after a total of eight hours at 950°C. The first 10 cm of the core were not analyzed for LOI as they were required for the measurements of short-lived radionuclides (^{210}Pb, ^{137}Cs and ^{241}Am).

Ten slabs were sub-sampled from core SCR1-18-01 and resin-embedded for analysis with a LEO Stereoscan 440 Leica (ASTRE platform of the Université Savoie Mont-Blanc) scanning electron microscope (SEM) with 20 kV tension, in order to qualify small scale sedimentary structures and grains at a 10 mm work distance. Chemical cartographies were performed on the slabs at a 23 mm work distance, using the Quantax EDX probe (Bruker) from the ASTRE platform, to highlight the elementary composition at the grain scale. The images were obtained in high vacuum mode, in secondary electron or backscattering electron modes.

3.4. Foraminifera analyses

A total of 35 samples were taken every 10 cm in fine-grained deposits and every 5 to 1 cm in coarse deposits, in core SCR1-18-01. Samples were weighed, dried at 60 °C and were sieved to retain the fractions 125-500 µm and > 500 µm. Foraminifera found in dried residues of the two size fractions were determined and taxa were identified using common taxonomical reference literature, describing the foraminifera in the Gulf of Mexico and the Caribbean Sea. All individuals were identified at least at a generic level, and their abundance was determined semi-quantitatively on the basis of the number of specimens observed in a single 6 x 10 cm picking tray filled with dry residue (Fig. 5): on a scale from 0 to 5: 0: barren sample; 1: 1 to 2 individuals; 2: 3 to 5 individuals; 3: 6 to 15 individuals; 4: 16 to 40 individuals; 5: more than 40 individuals. Only species occurrences with more than 6 individuals were considered as relevant.

3.5. Chronology

Short-lived radionuclides (^{210}Pb, ^{137}Cs and ^{241}Am) measurements were performed using the well-type germanium detectors at the Laboratoire Souterrain de Modane following methods outlined in Reyss et al. (1995). A total of 14 and nine samples were collected from cores SCR1-18-01 and SCR1-18-03, respectively, in the upper 12 cm and 10 cm, according to sedimentary facies boundaries. Excess ^{210}Pb was calculated as the difference between total ^{210}Pb and ^{226}Ra activities (Goldberg, 1963). Data were computed with the package '*serac*' in R software (Bruel and Sabatier, 2020).

A total of 13 organic macro-remains (wood and leaves) were collected in the muddy layers. ^{14}C measurements were performed by accelerator mass spectrometry (AMS) at the Poznan Radiocarbon Laboratory and at the Laboratoire de Mesure 14C (LMC14) ARTEMIS at the CEA (Atomic Energy Commission) Institute at Saclay. The ^{14}C ages were converted to 'calendar' years at two sigma using the Intcal13 calibration curve (Reimer et al., 2013). An age-depth model was constructed using the R code package 'clam' in R software (Blaauw, 2010), based on ^{14}C ages and on a historical hurricane occurrence, following Sabatier et al. (2012).

4. Results and interpretations

4.1. Facies description

For both cores SCR1-18-01 and SCR1-18-03, the sediment is composed of alternating coarse and fine units, with three main sedimentary facies identified. In the following, we mainly focus on core SCR1-18-01 and compare with samples of core SCR1-18-03.

Facies 1 (F1) consists of an organic-rich matrix with plant macro-remains such as wood and leaf fragments. The color of Facies 1 varies from dark brown to light yellowish brown, reflecting variations in the amount of organic matter. Some sediment layers show a green (olive) color due to the presence of algal mats (at 16 cm depth for example, Fig. 3). Mean organic matter (LOI550) content is 24% (+/- 8%) and mean carbonate (LOI950) content is 35% (+/- 2%) (Fig. 3). The carbonated fraction is composed of small calcitic shells and some patches of magnesian calcite (confirmed by the XRD data). These shells are about 0.5 to 1 mm-long and mainly consist of bivalves and benthic foraminifera, such as *miliolids* (Fig. 3), which are typical of tropical lagoon environments (Hallock and Glenn, 1986). Layers of facies 1 display varying amounts of *Miliolinella* sp. tests (0 to 5 on the semi-quantitative scale) that are thin, transparent and show only minimal amount of wear (Fig. 5). Facies 1 also contains very small (less than 5 µm in diameter) angular quartz grains (Fig. 3). Some rare thin horizontal beds of NaCl deposits (halite) are also visible (Fig. 3).

Facies 2 (F2) is a very pale brown unique deposit in the cores, between 46 and 40 cm depth in core SCR1-18-01, and from 31 to 23 cm depth in Core SCR1-18-03. It is composed of 8% (+/- 3%) organic matter (LOI550) and 42% (+/- 1%) carbonates (LOI950). It displays many whole and intact shells of variable sizes (0.5 mm to 1 cm) and some larger sandy grains (about 1 mm), the latter consisting of calcite and magnesian calcite (Fig. 3). Small bivalves (Fig. 3) and larger gastropod shells (around 1 cm long) are found. The gastropods were identified as *Cerithideopsis costata* (*da Coasta*, 1778), which are known to live in tropical brackish environments such as coastal lagoons (Reguero and Raz-Guzmán, 2018). The layer of facies 2 displays abundant individuals of *Miliolinella* sp. (2 to 5 on the semi-quantitative scale, Fig. 5), indicative of a tropical lagoon environment. Tests of *Miliolinella* sp. are thin, transparent and intact. Like facies F1, F2 contains very small quartz grains (Fig. 3). Halite (also evidenced by the XRD data) forms a coating around shells and sediment grains, and exhibits a typical cubic shape (Fig. 3).

Facies 3 (F3) displays a light gray or light yellowish brown color and consists of 40% (+/- 2%) carbonates (LOI950) and 9 (+/- 5) % organic matter (LOI550) (Fig. 3). The thickness of the F3 layers varies from less than 5 mm (65-64.5 cm depth) to 15 cm (61-46 cm depth) in core SCR1-18-01. However, in core SCR1-18-03 there are fewer and thinner layers of facies F3. Facies F3 is mainly composed of carbonated sand, largely derived from eroded fragments of marine skeletal material, including bivalves, molluscs and corals. Shell fragments are of variable size (100 to 1000 µm). Most F3 layers display a sharp contact with the underlying units and some layers present interbedded muddy layers or intraclasts. Both sand grains and shells consist of calcite and magnesium calcite (Fig. 3), but also of aragonite (based on XRD data). Layers of facies F3 display rare to abundant individuals of *Miliolinella* sp. (1 to 5 on the semi-quantitative scale, Fig. 5). Tests of *Miliolinella* sp. are thin, transparent and intact. However, all F3 samples contained some individuals (1 on the semi-quantitative scale, Fig. 5) of the larger, symbiont-bearing taxa *Amphistegina gibbosa* and *Archais angulatus* (Fig. 3). Some *Elphidium discoidale* (4 on the semi-quantitative scale) were also found between 92 and 93 cm depth in core SCR1-18-01 (Fig. 5). Unlike the specimens of *Miliolinella* sp., the tests of *Amphistegina gibbosa* and *Archais angulatus* are thick, heavily calcified, opaque and strongly abraded. These large

foraminifera represent larger symbiont-bearing species with a very robust shell, typical of high-energy reef environments (Hallock and Glenn, 1986).

In rare F3 layers, very few *Cerithideopsis costata* shells have been found. Based on the presence or absence of salt coating (halite) on grains, three sub facies are distinguished within F3: Subfacies 3.1 is characterized by salt coating around all grains; subfacies 3.2 is characterized by an absence of salt coating; subfacies 3.3 is characterized by both salt-coated and non-salt-coated grains (Fig. 3).

4.2. Geochemistry

The main results obtained from XRF analyses of core SCR1-18-01 are presented in Fig. 4. Linear regression tests on the Br and LOI550 results show a significant relationship with a R of 0.53 and p-value < 0.05 (0.01342). This suggests that Br XRF peak areas can probably be used as a proxy for organic matter content, since Br is known to have a strong affinity for organic matter (e.g., Chagué-Goff and Fyfe, 1996; Ribeiro Guevara et al., 2019). A strong relation between S and Br, in association with organic matter, has been previously reported using PCA, explaining 61% of the variance (Chagué et al., 2018). However, Br and S also occur in higher concentrations in seawater than freshwater (Wedepohl, 1971), and this could also explain their strong relationship in the Scrub lagoon, although it appears that their affinity with organic matter mostly explains their distribution.

The two first dimensions (Dim1 and Dim2) of the PCA (Fig. 4B) represent 67% of the total variance. Br, S, Fe and Si have a positive loading on Dim1 while Sr presents a negative correlation. Dim2 allows to distinguish Na and Cl (positive loading) from Ca with a negative correlation. From this PCA representation, four different endmembers can be identified: 1/ “salt” represented by Na and Cl, 2/ “organic matter” (OM) represented by Br and S, 3/ “silicate” represented by the Si and Fe and allochthonous inputs and 4/ “carbonates” endmembers represented by Ca and Sr. Ca and Sr do not exhibit a strong correlation and this can be explained by the presence of other minerals such as magnesian calcite.

By labelling samples with the facies information in the PCA, it was possible to establish a map of the geochemical data distribution (Fig. 4C). Facies F1 is dominated by the “organic matter”, “silicate”

endmembers and more or less influenced by the "salt" endmember. Facies F2 seems to be correlated with the "carbonates" endmember, due to the presence of Sr-rich shell fragments (e.g., Sabatier et al., 2010; Chagué-Goff et al., 2017 and references therein). Facies F3 is also linked to the "carbonates" endmembers (represented by Ca and Sr) and more or less influenced by the "salt" endmember. Moreover, facies F3 is hardly linked to the "organic matter" endmember represented mainly by the Br. Thus, facies F3 can be highlighted by the Sr/Br ratio, which increases in facies F3. (Fig. 5).

4.3. Grain size

Grain size results for core SCR1-18-01 are presented in Fig. 5. Denser layers highlighted by X-ray tomography data are characterized by a coarser grain size, and correspond to carbonated sand. The grain size contour plot shows that all these coarser layers have a similar grain size distribution with a mode around 800 µm (Fig. 5). Moreover, the Sr/Br ratio increases simultaneously with the grain size in F3 but presents a higher resolution than the grain size samples. This enable us to use Sr/Br as a high-resolution grain size proxy, which is useful to precisely identify the coarse deposits boundaries in the study area. Based on grain-size and Sr/Br ratio, 25 coarse layers (F3) were identified in core SCR1-18-01 and labelled L1 to L25.

4.4. Chronology

4.4.1. Short-lived radionuclides

Unfortunately, short-lived radionuclide results obtained from core SCR1-18-01 did not provide any interpretable information. For core SCR1-18-03, no sedimentation rate could be calculated on the basis of the ^{210}Pbex data. Nevertheless, the ^{210}Pbex profile shows that there is still some excess ^{210}Pb at 85 mm (Fig. 6), suggesting that sediment at this depth was deposited during the 20th century. Moreover, a clear peak in the ^{137}Cs profile at 17 mm depth (highest activity > 15 mBq/g) can be attributed to the maximum nuclear weapon tests in 1963 AD (Pennington et al., 1973). This suggests that F3 layer 25 (L#25 at 22 mm depth, Fig. 6) is probably older than 1963 AD. The deepest significant presence of ^{137}Cs activity, at 40 mm depth (5 mBq/g), could correspond to the first fallouts of nuclear weapon tests

in 1955 AD (Pennington et al., 1973). Thus, the youngest F3 layer (Layer 25, Fig. 5) in both cores was probably deposited between 1955 and 1963 AD (Fig. 6). Deeper L#24 and L#23 (Fig. 5) were probably deposited before 1955 AD but during the 20th century.

4.4.2. ^{14}C ages and age-depth model

The oldest age in core SCR1-18-01 is 464 +/- 74 cal AD at 105 cm depth (Table 2; Fig. 7). In Core SCR1-18-03, the oldest age is 1132 +/- 96 cal BC at 98.5 cm depth showing that the eastern part of the lagoon preserves a longer sediment record (Table 2; Fig. 7). A correlation between Core SCR1-18-01 and Core SCR1-18-03 was performed, based on F3 layers and using Sr/Br ratio and ^{14}C ages (Fig. 7).

An age-depth model was constructed for core SCR1-18-01 using the 10 ^{14}C ages (Table 2) and the information provided by the radionuclides (^{137}Cs peaks at 1963 AD and 1955 AD) (Fig. 6) for the topmost part of the core. First, the sediment depth of core SCR1-18-01 was corrected by subtracting the 25 F3 layers, which were interpreted as "instantaneous" events, in order to build an event-free sedimentary record (Fig. 8A) (Sabatier et al., 2017). Then, an age-depth model was calculated by a smooth spline function using the R package *Clam* (Blaauw, 2010). The vertical blue bars (Fig. 8B) represent the ages of the 25 "instantaneous" deposits with uncertainties (2s) resulting from the age model. The mean sedimentation rate (without "instantaneous" deposits) is 0.47 +/- 0.24 mm yr^{-1}.

5. Discussion

5.1. Sedimentary facies interpretation

Sedimentary facies **F1** consists of mostly silty brown deposits, which contain only one single taxon of *Miliolinella sp.*. Miliolids are known to be particularly tolerant for increased salinity (Murray, 2006) and assemblages strongly dominated by miliolids are typically found in hypersaline lagoons. Thus they most likely represent the autochthonous fauna of the lagoon. This facies is also rich in organic matter, Br and S ("Organic Matter" endmember, Fig. 4B). This high organic matter content is probably related

to autochthonous algal productivity as terrestrial organic matter inputs through run-off reaching the lagoon from the inner part of this small karstic island is very limited.

The very small angular quartz grains found in the organic matrix are unlikely to originate from Scrub Island, which only comprises carbonates. Both the grain size and morphology can be interpreted as the result of fragmentation of larger quartz grains. Moreover, the angular quartz grains suggest that they have been transported in suspension, without an erosive rolling/saltation phase (Coude-Gaussen, 1991). Furthermore, the very small mean grain size (< 5 µm) may indicate an aeolian transport, far away from the source, as reported by Van der Does et al. (2016). Therefore, we interpret these grains as long-range-transported (LRT) aeolian particles, transported from the Saharan desert to this island. African dust is already known to be transported to the Caribbean, at least as far as Florida (Prospero, 2003; Muhs et al., 2007; Muhs and Budahn, 2009; Muhs et al., 2012). The Saharan dust includes other particles such as clays and iron oxides (Coude-Gaussen, 1991; Muhs et al., 2012). The strong positive correlation between Fe and Si on the PCA (Fig. 4B) suggests that Fe in F1 most probably had the same aeolian origin ("silicates" endmember, Fig. 4B). These two poles are the major components of facies F1 (Fig. 4C). Based on these data, sedimentary facies F1 is interpreted as recording both the autochthonous lagoon sedimentation and probably aeolian sediment inputs.

Sedimentary facies **F3** consists of 25 layers of carbonated sand with mostly aragonitic shell fragments. These layers are plotting close to the "carbonates" endmembers (Fig. 4B) with high Ca and Sr contents found in primary marine carbonate minerals, including aragonite and high-Mg calcite. Since Br is associated with autochthonous organic matter in this lagoon, the synchronous variations of Sr/Br ratio and grain-size increase are used to identify these 25 layers (Fig. 5). Eleven intervals of facies 3 (Fig. 5) display large symbiont-bearing foraminifera *A. gibbosa* and *A. angulatus*, which are typical of open marine subtropical to tropical environments with a normal salinity. Based on their living environment and their abraded tests, it is likely that these taxa are allochthonous and that they were transported in the lagoon during marine incursions (e.g., Pilarczyk et al., 2016). Most F3 layers exhibit a sharp basal

424 contact and thin inland, with the number of these units also decreasing landward as attested from core
425 correlation (Fig. 7). Consequently, F3 layers are interpreted as high-energy deposits resulting from
426 overwash of the sandy barrier related to either hurricanes or tsunamis.
427
428 Sedimentary facies F**2** (46 to 40 cm depth) is the only one showing large accumulations of intact
429 *Cerithideopsis costata* shells associated with small bivalve shells. The large amount of shells explains
430 the high counts of Sr for the "carbonates" endmember. This shell accumulation is found at the same
431 period (1450-1635 AD) in both cores (Fig. 7), suggesting that it probably extended in the entire lagoon.
432 It could record a change in physical or chemical parameters inside the lagoon. The thickest F3 sandy
433 layer (L#14, 61 to 47 cm depth in core SCR1-18-01) occurs just below facies F2, and was identified in
434 core SCR1-18-03 (41 to 38 cm depth). Two hypotheses may explain such accumulation of
435 *Cerithideopsis costata* shells in the lagoon. First, we assume that the massive sand accumulation
436 revealed bay L#14 led to drastic changes in quantity and quality of sedimentary organic matter, sulfide
437 contents, and sediment redox condition, compared to normal organic rich sediment (facies F1) as also
438 reported in a shallow eutrophic lagoon from Sendai Bay in Japan (Kanaya et al., 2015). Such changes
439 in the habitat quality may explain the development of *Cerithideopsis costata*. According to the
440 radiocarbon ages (Table 2), this change in macrozoobenthic assemblage lasted 200 years after the
441 massive sand input and before the deposition of the next facies F1 layer. The second hypothesis is that
442 the F3 deposit (Layer 14) could correspond to a high-energy event that may have breached the sand
443 barrier causing the level of the lagoon to drop. A low water level would have resulted in a salinity
444 increase in the lagoon. Indeed, Facies 2 displays high concentration of halite around the shells (Facies
445 2) (Fig. 3). Following this hypothesis, salinity would have become too high for *Cerithideopsis costata,*
446 that develop in brackish water, leading to the death of the individuals and accumulation of their shells
447 in the lagoon during this period.
448
449 **5.2. Limitations of the study site for paleo tsunami and paleo hurricane chronicles**

Since F3 layers are probably sediment records of high-energy marine flooding, the studied lagoon seems to represent an ideal site for recording past tsunamis or hurricanes. Today the sandy barrier separating the lagoon from the open ocean is 2 to 5 m-high from north to south. Therefore, a maximum wave height over 2 to 5 m is needed to overwash or overtop the dune crest. Such a runup may result from exceptionally high sea levels (e.g., Atwater et al., 2014) reached during hurricanes, due to the combined effects of storm surge (resulting from low pressure effect and wind stress), wave setup, swash and infra gravity waves (e.g., Chaumillon et al., 2017). Alternatively, runups higher than 2 to 5 m may also occur during tsunamis (e.g., Atwater et al., 2012). The sensitivity of a given barrier to overwash may vary through time because of many factors that can be grouped as allogenic and autogenic (Scileppi and Donnelly, 2007). One major allogenic parameter corresponds to sea level variations, since sea level rise increases the vulnerability of barriers to overwash. However, no major sea level changes have been reported over the last 1600 years in the Antilles (Khan et al., 2017). Autogenic parameters, including the presence or absence of an inlet or a breach also control the barrier sensitivity to overwash (Donnelly et al., 2001; Sabatier et al., 2012). The sensitivity of a lagoon system to record a hurricane and/or a tsunami increases when the barrier is breached or cut by an inlet. After an overwash, barrier breach and/or lowering of the barrier may occur for a limited period of time and lead to a greater vulnerability to future overwash. It is very likely that the barrier morphology has evolved during the past 1600 years (e.g., Atwater et al., 2012). However, we do not have any constraints about such evolution, thus reconstruction of paleo intensities from the sediment records in the studied lagoon remains difficult. Indeed, estimating the frequency of marine-flooding sediment records from coarse sediment layers (F3 layers) must be done with caution. In fact, every F3 layer does not necessary correspond to a single short-term event. For example, if two such events occurred in a short period of time, this may lead to the deposition of two amalgamated sandy layers that cannot be differentiated. On the other hand, very high energy events may erode lagoon sediments, including previously deposited event layers, as reported on the Sendai Plain during the 2011 Tohoku-oki tsunami (Shinozaki et al., 2015). Thus, this cannot be completely discounted, although it is also possible that the frequency of high energy events is close to the frequency of sand layers recorded on Scrub Island.

5.3. Processes involved in high energy events

F3 high-energy deposits may either record hurricane or tsunami events. Hurricane and tsunami deposits mostly result from onshore transport of near-shore sediment and exhibit a number of similar characteristics (e.g., Morton et al., 2007). Many criteria have already been defined to distinguish tsunami from storm deposits (e.g., Goff et al., 2004 ; Morton et al., 2007 ; Engel et al., 2016 ; Kusumoto et al., 2018), however, these criteria are most of the time site-dependent. Among the 25 F3 deposits, two deposits display specific criteria which may contribute to their identification as tsunami records.

5.4. Tsunami deposits

The upper layer displaying specific criteria corresponds to layer 17 (L#17, Fig. 5). It is 4 cm thick in core SCR1-18-01. L#17 is also recorded in Core SCR1-18-03 (Fig. 7). L#17 is composed of a sandy layer with a mud layer at the top. The sandy part displays an upward small grain size decrease (530 to 470 µm), which most likely indicates that the sediment fell out of suspension (e.g., Morton et al., 2007). An intraclast, which is a rip up clast of the underlying cohesive substrate (facies F1), is visible in the sand layer (Fig. 3). Such feature occurs when the underlying deposit is eroded by the high energy flow and suspended in the water before being deposed, when the flow speed decreases (e.g., Morton et al., 2007). These characteristics are commonly used to identify tsunami deposits and thus have led us to interpret L#17 as a tsunami deposit.

Moreover, L#17 does not display salt-coated grains. Considering tsunami waves have longer wavelengths than hurricanes waves, tsunami deposits often contain records of deeper reworked sediment (Uchida et al., 2010).Variations of salt coating around grains (subfacies 3.1, 3.2 and 3.3, Fig. 3) could be a potential marker of the origin of sediment reworked by marine flooding. Salt coatings may result from halite precipitation on sand grains exposed to both sea spray /sea water and strong evaporation. Such conditions are commonly found on beach barriers (e.g., Ward, 1967) but also on land following tsunami inundation (e.g., Chagué-Goff et al., 2012), even one year after the event despite dilution by rainfall (Chagué-Goff et al., 2014), due to capillary action. Thus, abundance of salt coating could be an indicator of beach barrier sands. On the contrary, the absence of salt coatings can be related to an absence

505 of strong evaporation, a situation which can be found in submarine sand, or sand from the lower
506 shoreface (e.g., Ward, 1967). Thus, the absence of salt coating on grains in L#17 might indicate a deeper
507 sediment source, farther away from the shoreline. Even though post-depositional processes should also
508 be considered, the covering of sandy deposits by the fine grained facies 1 allows the preservation of
509 halite coatings on the sandy grains.

510 Finally, the 2 cm thick mud layer above the sand deposit contains a large amount of wood and
511 vascular plant remains. This concentration of plant remains shows an important terrestrial input in the
512 lagoon that can be interpreted as resulting from the backwash during the L#17 event. Alternatively, this
513 concentration in plants remains could also be due to the incorporation of vegetation eroded from the
514 sand barrier by the tsunami wave. As organic matter is less dense, it is deposited on top of the tsunamis
515 deposit out of suspension, as previously reported (e.g., Chagué-Goff et al., 2011).

516

517 According to the age model (Fig. 8), this event is dated at 1720 cal. AD (1652-1810 cal. AD),
518 which could correspond to the 1755 AD Lisbon tsunami (Chester, 2001). Although originating in the
519 Eastern Atlantic, this tsunami was able to reach Scrub Island lagoon, which is oriented towards the west.
520 This could be explained by local tsunami amplification due to the shallow bathymetry of the area and
521 the interconnected channel between Anguilla and Scrub, with for example a resonant amplification of
522 the tsunami waves between Anguilla and Scrub (e.g., Munger and Cheung, 2008).

523

524 Layer L14 (L#14, Fig. 5) is the older layer displaying specific criteria. First, it is the thickest
525 (14 cm thick in SCR1-18-01) among all the F3 layers in both cores (Fig. 7), possibly indicating the
526 occurrence of an exceptional marine incursion. It is composed of a massive single sandy bed. The
527 absence of grain size variations is indicative of an extremely rapid deposition such as would occur when
528 flow decelerates between the uprush and backwash phases during a tsunami (Morton et al., 2007).
529 However, the CT image (Fig. 5) displays some internal mud laminae at 57.5 and 59 cm depth. These
530 layers are related to the suspension load during the waning stage between waves, with sufficient time
531 for mud to settle between successive waves (Jaffe et al., 2003; Naruse et al., 2010). L#14 shows a mix
532 of salt coated and non-salt coated grains, probably indicating sediment reworked from both the barrier

and the shoreface. Thus, these criteria have led us to interpret this deposit as the result of a major tsunami event. Finally, the presence of the single facies F2 deposit just above L#14 suggests that this event was the only one able to have a long-term environmental impact (changes in nutrient inputs and/or salinity for 200 years) inside the lagoon over the last 1600 years BP, reinforcing the hypothesis of an exceptional event.

L#14 is dated at 1415 cal. AD (1364-1469 cal. AD). By comparison with others studies in the Caribbean region, this age corresponds to the late Middle Age event identified in St Thomas (US Virgin Islands) dated between 1200 and 1450 cal. AD (Fuentes et al., 2017) but also in Anegada (British Virgin Islands), where it was dated between 1200 and 1480 cal. AD (Atwater et al., 2017). These two islands are located between 150 and 200 km northwest from Scrub Island, close to the seismically active Puerto Rico Trench (Fig. 1B), which is a possible source for a tsunami in the Caribbean (Atwater et al., 2017). In Bonaire (south Caribbean) sublittoral sediments interrupting onshore sedimentary sequences on the eastern shore (Boka Washikemba), provided evidence for a major wave impact shortly before 500 cal. BP (1450 cal. AD), which most likely corresponds to a tsunami (Engel et al., 2010). In the same region, the study of a sediment core from a saline lagoon on Cayo Sal Island, (western Venezuela) showed probably tsunami-laid reworked peat (Weiss, 1979). This event is dated between 1180 and 1450 AD (Weiss, 1979), which correspond to an age between 1046 and 1481 cal AD (Reimer et al., 2013). These two islands are more than 800 km south from the Puerto Rico Trench, indicating that if all the study sites cited above recorded the same tsunami, it most probably hit the whole Caribbean area.

It is also possible that coarse layers dated to the expected age of this tsunami in other study sites have been misinterpreted as hurricane or storm events, such as in St-Martin 25 km from Scrub Island, within a lagoon with the same orientation (Malaizé et al., 2011) or in Vieques, Puerto Rico with a single high energy event during a period with fewer intense hurricane strikes (Donnelly and Woodruff, 2007) or in Belize where the event was described as "much stronger than all other storms in the record" (McCloskey and Keller, 2009). If all the above-cited sediment records are related to the same event, their wide geographical extent would exclude the hypothesis of a hurricane record, as one hurricane generally cannot cross both the north and south of the Caribbean. Finally, while most of these studies

proposed an age for this event with a more than a 200-year uncertainty, the new age constrain provided by our age model gives a much more accurate age with only a 100-year uncertainty. The identification of new sedimentary records of this event would therefore provide an opportunity to further refine its chronology and source. A record of this event might be preserved in others islands in the northern or southern Caribbean and it should be investigated.

5.5. Hurricane chronicle and climate forcing

If layers L#14 and L#17 are related to tsunami events, the 23 remaining sandy layers (F3 deposits) deposited in the studied lagoon over the last 1600 years, can probably be interpreted as resulting from storms/hurricanes (Fig. 8). Among those 23 layers, the three most recent F3 deposits occurred since the mid-19th century and can be associated with historical hurricanes. Intriguingly only three high-energy events are recorded in the lagoon as sandy layers, while 13 hurricane trajectories (Table 1) passed less than 30 km from Scrub Island since 1852 AD (coast.noaa.gov/hurricanes, 2020). Thus, we assume that Scrub lagoon has only recorded the closest and most intense hurricanes.

According to ^{137}Cs activities, L#25 was deposited between 1955 (first ^{137}Cs fallouts) and 1963 AD (maximum nuclear weapon test in the Northern Hemisphere, Fig. 6). This layer can be tentatively related to the only hurricane that passed within 30 km from Scrub between 1955 and 1963, the Category 3 Hurricane Donna, which took place in 1960 AD (Table 1, coast.noaa.gov/hurricanes, 2020). According to the short-lived radionuclide measurements, L#24 occurred before 1955 AD but during the 20th century, as the sediment still presents ^{210}Pbex activities (Fig. 6), and based on our age model, it is dated between 1935 and 1959 AD (Fig. 8). There were two hurricanes in the region during this period: Category 3 Hurricane Dog (1950) and Category 1 Hurricane Alice (1955) (Table 1). As Dog seems to be both closer and stronger than Alice, it may be recorded by L#24. L#23 is dated between 1903 and 1957 AD with the best age being 1930 AD according to the age model (Fig. 8). L#23 can be attributed to the unnamed category 3 hurricane that occurred in 1922 AD (Table 1).

Based on the instrumental data available, it appears that three conditions must be fulfilled for a given hurricane to leave a sedimentary record in the studied lagoon, assuming enough sediment

availability: (1) at least category 3 on the Saffir-Simpson scale, (2) a hurricane track less than 30 km from Scrub Island and (3) a hurricane heading southward of Scrub and northwest of Anguilla (Fig. 2). It is likely that the hurricane path must face the barrier to be recorded in the lagoon and thus must reach northwest Anguilla, as Anguilla Island appears to act as a barrier for hurricanes passing south of the island. This could explain why Category 5 Hurricane Irma and Category 3 Hurricane Lenny were not recorded in the studied lagoon, as their path bypassed Anguilla from the south (Fig. 2). Moreover, hurricanes passing north of the lagoon cannot be recorded.

The studied lagoon provides an opportunity to estimate long term hurricane activity in the region over the last 1600 years. A 101-year window event frequency was made for Scrub Lagoon (Fig. 9D) based on the chronology of the hurricane deposits in the sediment record. Six time periods are characterized by more frequent hurricane sediment records (at least two per century): 445-525, 720-835, 1080-1230, 1625-1695, 1745-1890 and 1920-1970 cal AD (Fig. 9D). The longest period with a relative high frequency of hurricanes (1080-1230 AD) occurred during the Medieval Warm Period (800-1300 AD). It is known that during this period, the sea surface temperatures (SSTs) were high in the Atlantic Main Development Region of hurricanes (MDR), which extends in the east from Cape Verde to Guinea in Africa, to the Caribbean Sea in the west (Wallace et al., 2019). Murakami et al. (2018) showed that high frequency hurricanes periods seems to be linked to warm SSTs in the tropical North Atlantic, as hurricanes obtain more energy from warmer oceans during their westward propagation from the MDR. On the other hand, five time periods are characterized by an absence of hurricane in the sediment record: ~560, ~670, 965-1020, 1400-1600, ~1740 cal AD (Fig. 9D). The longest period without hurricane (1400-1600 AD) occurred during the first part of the Little Ice Age (1450-1900 AD), when the SSTs where low in the Atlantic Ocean (Wallace et al., 2019). However, the period with the highest frequency also occurred from 1740 to 1890 cal AD, when SSTs are supposed to be low in the Atlantic Ocean. Burn et al. (2016) showed that in Barbuda Island (Fig. 1), El Niño Southern Oscillation (ENSO) combined with the Atlantic Multidecadal Oscillation (AMO) appear to have exerted some additional influence on the rainfall activity from 1720 to 1860 cal AD, which could indicate the influence of these parameters

616 in the Lesser Antilles and may explain the singularity of the increase in the hurricane frequency in Scrub
617 Island during this period.
618
619 Scrub Island sediment record brings new knowledge about variations in past hurricane activity
620 in the Caribbean. Thus we compared this new chronicle to other sites where hurricane sediment records
621 are available: A/ Salt Pond, Massachusetts (Donnelly et al., 2015), B/ South Andros, Bahamas (Wallace
622 et al., 2019), C/ Lighthouse Reef blue hole, Belize (Denommee et al., 2015) (Fig. 9A, B, C). From this
623 comparison (Fig. 9), it appears that Scrub and South Andros (Bahamas) records are in phase, except
624 from a short period between 900 and 1050 cal AD and at lesser extend between 1230 to 1500 cal AD
625 with an increase in the Bahamas hurricane chronicle. On the other hand, the Long Pond (Massachusetts,
626 USA) signal is in antiphase with Scrub Island, except from 445 to 525 cal AD, where storm frequency
627 increases in both sites, but with a larger increase for Long Pond. The signal in the Lighthouse Reef blue
628 hole (Belize) is mostly not in phase with the Scrub Island signal, except for the periods 1400-1600 and
629 1920-1970 cal AD.
630 Differences in hurricane sediment records between Scrub Island and the others sites can be
631 partially explained by the position of Scrub Island with respect to hurricane tracks. Compared to the
632 three other sites, Scrub Island is the most eastern one, located at the forefront of many hurricane
633 trajectories heading westward to the northern part of Gulf of Mexico/Caribbean. Among the 13 historical
634 hurricanes that passed within 30 km from Scrub, two also hit the Bahamas, two headed towards Belize
635 but did not reach this area and most of them have made their way close to the American East coast but
636 never reached the Massachusetts region (Fig. 9). Nevertheless, even if this regional comparison provides
637 a relative coherent pattern, small differences of hurricane activity between each site could be also
638 explained by the hurricane intensity changes between Scrub Island and the other sites and by the long
639 term sensitivity variations of the different sedimentary systems for recording hurricanes.
640
641 However, the antiphase signal of the Massachusetts with respect to the three other sites may provide
642 evidence of a latitudinal forcing for the hurricane tracks. Thus, Wallace et al. (2019) showed that periods
643 of intense hurricane activity in the Bahamas correspond to a position further north of the ITCZ (Haug

644 et al., 2001) (Fig. 9B, E), except for the 640-815 cal AD period. For the Scrub Island signal, some
645 periods (445-525 and 1745-1840 cal AD) with numerous hurricane sediment records, correspond to a
646 northern position of the ITCZ (Fig. 9D, E), which is consistent with the Bahamas signal. However, other
647 periods high hurricane record in Scrub Island correspond to a more southern ITCZ position (720-835,
648 1080-1230 and 1625-1695 cal AD, Fig. 9, D, E) showing that for the Scrub Island signal, the
649 correspondence between the ITCZ position and the hurricane activity intensification is not obvious.
650 Thus, other climatic forcing parameters are expected to influence hurricane tracks. Therefore, it is
651 necessary to investigate other sites in the Caribbean in order to better understand climatic parameters
652 modulating the trajectory of hurricanes.
653

654 # 6. Conclusion

655 Using sedimentological, geochemical, microfaunal and chronological analyses of two cores
656 from a small coastal lagoon on Scrub Island in the north eastern Caribbean region, we identified 25
657 marine-sourced sand layers alternating with lagoon deposits. These sand layers most probably result
658 from high-energy marine flooding related to tsunami or hurricane events.

659 Based on sedimentological criteria and correlations with already published data, two of these 25
660 sand layers were interpreted as tsunami deposits. The most recent presenting intraclasts and a mud drape
661 is associated with the transatlantic tsunami that was generated by the 1755 AD Lisbon earthquake
662 already recorded in many Caribbean islands. The oldest is the thickest homogenous sandy layer recorded
663 in the lagoon and dated at 1415 cal. AD (1364-1469 cal. AD). It displays two internal mud laminae,
664 related to the suspension load of the waning stage between waves. Published studies in the Caribbean
665 region suggest that this event has left a sedimentary record in other islands, although sometime
666 interpreted as a hurricane. As this event was recorded in both the northern and the southern part of the
667 Caribbean, its large extent supports a tsunamigenic source. The presence or absence of salt coating on
668 sand grains, indicating a barrier or lower shoreface origin for sand grains, respectively, could be used as
669 a new criterion to distinguish tsunami (reworking both barrier and shoreface sediments) from hurricane
670 (mostly reworking barrier sediments) deposits.

671 The 23 remaining sandy layers were interpreted as resulting from hurricanes. The chronology
672 established with short lived radionuclides suggests that the three most recent deposits were associated
673 with historical hurricanes and it appears that three conditions must be fulfilled for a given hurricane to
674 leave a record in the studied lagoon: (1) at least category 3 on the Saffir-Simpson scale, (2) a storm track
675 at less than 30 km from Scrub Island and (3) a storm track located southwestward with respect to the
676 studied lagoon.

677 The studied sedimentary sequence provides an opportunity to explore the past hurricane activity
678 in the region over the last 1600 years. Six periods of increase in hurricane frequency and five periods
679 without hurricane events are suggested. Those variations in hurricane frequency are similar to the
680 variations recorded in the Bahamas and are in antiphase with the Massachusetts (USA) hurricane
681 chronicle, which could provide evidence of a latitudinal forcing for the hurricane tracks through time.
682 The position of the ITCZ has already been proposed as a forcing parameter modulating the hurricane
683 tracks but as its relation with the Scrub Island chronicle is not obvious, other climatic forcing parameters
684 are probably involved.

685 Finally, the position of Scrub lagoon sediment-fill in the north eastern part of the Caribbean area
686 provides a new and unique sedimentary record of both tsunamis and hurricanes, and this study helps
687 gain a better understanding of the long-term climate and geodynamic history of this region particularly
688 vulnerable to those destructive events.

689

Acknowledgements

This work is part of the CARQUAKES project (ANR-17-CE03-0006). The objective of the CARQUAKES project is to improve the catalog of large earthquakes and tsunamis in the Lesser Antilles and characterize the related hazards by applying an innovative and novel multidisciplinary approach combining several state-of-the-art methods of offshore and onshore paleoseismology and tsunami modelling.

^{14}C analyses were acquired thanks to the CNRS-INSU ARTEMIS national radiocarbon AMS measurement programme at Laboratoire de Mesure 14C (LMC14) in the CEA Institute at Saclay (French Atomic Energy Commission). The authors thank the Laboratoire Souterrain de Modane (LSM) facilities for the gamma spectrometry measurements and Environnement, Dynamique et Territoires de Montagne for the X-ray fluorescence analyses.

The Lidar DEM of Anguilla is a courtesy of the Government of Anguilla (Department of Disaster Management) for academic research projects dedicated to seismic and tsunami hazard in Anguilla.

We thank the skipper Nicolas Jammes, who was involved in the March 2018 field survey.

References

Atwater, B.F., 1987. Evidence for Great Holocene Earthquakes Along the Outer Coast of Washington State. Science 236, 942–944. https://doi.org/10.1126/science.236.4804.942

Atwater, B.F., Fuentes, Z., Halley, R.B., Ten Brink, U.S., Tuttle, M.P., 2014. Effects of 2010 Hurricane Earl amidst geologic evidence for greater overwash at Anegada, British Virgin Islands. Advances in Geosciences 38, 21–30. https://doi.org/10.5194/adgeo-38-21-2014

Atwater, B.F., ten Brink, U.S., Buckley, M., Halley, R.S., Jaffe, B.E., López-Venegas, A.M., Reinhardt, E.G., Tuttle, M.P., Watt, S., Wei, Y., 2012. Geomorphic and stratigraphic evidence for an unusual tsunami or storm a few centuries ago at Anegada, British Virgin Islands. Natural Hazards 63, 51–84. https://doi.org/10.1007/s11069-010-9622-6

Atwater, B.F., ten Brink, U.S., Cescon, A.L., Feuillet, N., Fuentes, Z., Halley, R.B., Nuñez, C., Reinhardt, E.G., Roger, J.H., Sawai, Y., Spiske, M., Tuttle, M.P., Wei, Y., Weil-Accardo, J., 2017. Extreme waves in the British Virgin Islands during the last centuries before 1500 CE. Geosphere 13, 301–368. https://doi.org/10.1130/GES01356.1

Baldini, L.M., Baldini, J.U.L., McElwaine, J.N., Frappier, A.B., Asmerom, Y., Liu, K., Prufer, K.M., Ridley, H.E., Polyak, V., Kennett, D.J., Macpherson, C.G., Aquino, V.V., Awe, J., Breitenbach, S.F.M., 2016. Persistent northward North Atlantic tropical cyclone track migration over the past five centuries. Scientific Reports 6. https://doi.org/10.1038/srep37522

Baumann, J., 2017. Signature sédimentaire des submersions de tempête dans le domaine rétrolittoral : application à la Charente Maritime (phdthesis). Université de La Rochelle.

Bernard, P., Lambert, J., 1988. Subduction and seismic hazard in the northern Lesser Antilles: Revision of the historical seismicity. Bulletin of the Seismological Society of America 78, 1965–1983.

Blaauw, M., 2010. Methods and code for 'classical' age-modelling of radiocarbon sequences. Quaternary Geochronology 5, 512–518. https://doi.org/10.1016/j.quageo.2010.01.002

Boudon, G., Friant, A.L., Komorowski, J.-C., Deplus, C., Semet, M.P., 2007. Volcano flank instability in the Lesser Antilles Arc: Diversity of scale, processes, and temporal recurrence. Journal of Geophysical Research: Solid Earth 112. https://doi.org/10.1029/2006JB004674

732 Bruce, A., 2000. Anguilla. Geology Today 16, 112–114. https://doi.org/10.1046/j.1365-
733 2451.2000.00007.x
734 Bruel, R., Sabatier, P., 2020. Serac: a R package for ShortlivEd RAdionuclide Chronology of recent
735 sediment cores. 38. https://doi.org/10.31223/osf.io/f4yma
736 Burn, M.J., Holmes, J., Kennedy, L.M., Bain, A., Marshall, J.D., Perdikaris, S., 2016. A sediment-based
737 reconstruction of Caribbean effective precipitation during the 'Little Ice Age' from Freshwater
738 Pond, Barbuda. The Holocene 26, 1237–1247. https://doi.org/10.1177/0959683616638418
739 Cangialosi, J. P., Latto, A. S., Berg, R., 2018. National Hurricane Center tropical cyclone report:
740 Hurricane Irma. NOAA/NWS Rep. AL112017, 111 pp.
741 Chagué, C., Sugawara, D., Goto, K., Goff, J., Dudley, W., Gadd, P., 2018. Geological evidence and
742 sediment transport modelling for the 1946 and 1960 tsunamis in Shinmachi, Hilo, Hawaii.
743 Sedimentary Geology 364, 319–333. https://doi.org/10.1016/j.sedgeo.2017.09.010
744 Chagué-Goff, C., 2010. Chemical signatures of palaeotsunamis: A forgotten proxy? Marine Geology
745 271, 67–71. https://doi.org/10.1016/j.margeo.2010.01.010
746 Chagué-Goff, C., Fyfe, W.S., 1996. Geochemical and petrographical characteristics of a domed bog,
747 Nova Scotia: a modern analogue for temperate coal deposits. Organic Geochemistry, The
748 Society for Organic Petrology 24, 141–158. https://doi.org/10.1016/0146-6380(96)00014-9
749 Chagué-Goff, C., Niedzielski, P., Wong, H.K.Y., Szczuciński, W., Sugawara, D., Goff, J., 2012.
750 Environmental impact assessment of the 2011 Tohoku-oki tsunami on the Sendai Plain.
751 Sedimentary Geology, The 2011 Tohoku-oki tsunami 282, 175–187.
752 https://doi.org/10.1016/j.sedgeo.2012.06.002
753 Chagué-Goff, C., Schneider, J.-L., Goff, J.R., Dominey-Howes, D., Strotz, L., 2011. Expanding the
754 proxy toolkit to help identify past events — Lessons from the 2004 Indian Ocean Tsunami and
755 the 2009 South Pacific Tsunami. Earth-Science Reviews, The 2009 South Pacific tsunami 107,
756 107–122. https://doi.org/10.1016/j.earscirev.2011.03.007
757 Chagué-Goff, C., Szczuciński, W., Shinozaki, T., 2017. Applications of geochemistry in tsunami
758 research: A review. Earth-Science Reviews 165, 203–244.
759 https://doi.org/10.1016/j.earscirev.2016.12.003

760 Chagué-Goff, C., Wong, H.K.Y., Sugawara, D., Goff, J., Nishimura, Y., Beer, J., Szczuciński, W., Goto,
761 K., 2014. Impact of Tsunami Inundation on Soil Salinisation: Up to One Year After the 2011
762 Tohoku-Oki Tsunami, in: Kontar, Y.A., Santiago-Fandiño, V., Takahashi, T. (Eds.), Tsunami
763 Events and Lessons Learned: Environmental and Societal Significance, Advances in Natural
764 and Technological Hazards Research. Springer Netherlands, Dordrecht, pp. 193–214.
765 https://doi.org/10.1007/978-94-007-7269-4_10
766 Chaumillon, E., Bertin, X., Fortunato, A.B., Bajo, M., Schneider, J.-L., Dezileau, L., Walsh, J.P.,
767 Michelot, A., Chauveau, E., Créach, A., Hénaff, A., Sauzeau, T., Waeles, B., Gervais, B., Jan,
768 G., Baumann, J., Breilh, J.-F., Pedreros, R., 2017. Storm-induced marine flooding: Lessons from
769 a multidisciplinary approach. Earth-Science Reviews 165, 151–184.
770 https://doi.org/10.1016/j.earscirev.2016.12.005
771 Chester, D.K., 2001. The 1755 Lisbon earthquake. Progress in Physical Geography: Earth and
772 Environment 25, 363–383. https://doi.org/10.1177/030913330102500304
773 Cordrie, L., Escartin, J., Gailler, A., Feuillet, N., Heinrich, P., 2019. Simulation of the 2004 tsunami of
774 Les Saintes in Guadeloupe (Lesser Antilles), in: oceans 2019 - Marseille. Presented at the
775 OCEANS 2019 - Marseille, IEEE, Marseille, France, pp. 1–9.
776 https://doi.org/10.1109/OCEANSE.2019.8867447
777 Coude-Gaussen, G., 1991. Les poussières sahariennes. Cycle sédimentaire et place dans les
778 environnements et paléoenvironnements désertiques. Sciences Géologiques. Bulletin, tome 44,
779 n°3-4, 1991. Les massifs anciens de France - II, sous la direction de Alain Piqué. 44.
780 DeMets, C., Jansma, P.E., Mattioli, G.S., Dixon, T.H., Farina, F., Bilham, R., Calais, E., Mann, P., 2000.
781 GPS geodetic constraints on Caribbean-North America Plate Motion. Geophysical Research
782 Letters 27, 437–440. https://doi.org/10.1029/1999GL005436
783 Denommee, K.C., Bentley, S.J., Droxler, A.W., 2015. Climatic controls on hurricane patterns: a 1200-
784 y near-annual record from Lighthouse Reef, Belize. Scientific Reports 4.
785 https://doi.org/10.1038/srep03876

786 Donnelly, J.P., Hawkes, A.D., Lane, P., MacDonald, D., Shuman, B.N., Toomey, M.R., van Hengstum,
787 P.J., Woodruff, J.D., 2015. Climate forcing of unprecedented intense-hurricane activity in the
788 last 2000 years: Donnelly et al. Earth's Future 3, 49–65. https://doi.org/10.1002/2014EF000274
789 Donnelly, J.P., Smith Bryant, S., Butler, J., Dowling, J., Fan, L., Hausmann, N., Newby, P., Shuman,
790 B., Stern, J., Westover, K., Webb III, T., 2001. 700 yr sedimentary record of intense hurricane
791 landfalls in southern New England. Geological Society of America Bulletin 113, 714–727.
792 https://doi.org/10.1130/0016-7606(2001)113<0714:YSROIH>2.0.CO;2
793 Donnelly, J.P., Woodruff, J.D., 2007. Intense hurricane activity over the past 5,000 years controlled by
794 El Niño and the West African monsoon. Nature 447, 465–468.
795 https://doi.org/10.1038/nature05834
796 Dorel, J., 1981. Seismicity and seismic gap in the Lesser Antilles arc and earthquake hazard in
797 Guadeloupe. Geophysical Journal of the Royal Astronomical Society 67, 679–695.
798 https://doi.org/10.1111/j.1365-246X.1981.tb06947.x
799 Dunn, G.E., 1961. The Hurricane season of 1960. Monthly Weather Review.
800 Engel, M., Brückner, H., Fürstenberg, S., Frenzel, P., Konopczak, A.M., Scheffers, A., Kelletat, D.,
801 May, S.M., Schäbitz, F., Daut, G., 2013. A prehistoric tsunami induced long-lasting ecosystem
802 changes on a semi-arid tropical island—the case of Boka Bartol (Bonaire, Leeward Antilles).
803 Naturwissenschaften 100, 51–67. https://doi.org/10.1007/s00114-012-0993-2
804 Engel, M., Brückner, H., Wennrich, V., Scheffers, A., Kelletat, D., Vött, A., Schäbitz, F., Daut, G.,
805 Willershäuser, T., May, S.M., 2010. Coastal stratigraphies of eastern Bonaire (Netherlands
806 Antilles): New insights into the palaeo-tsunami history of the southern Caribbean. Sedimentary
807 Geology 231, 14–30. https://doi.org/10.1016/j.sedgeo.2010.08.002
808 Engel, M., Oetjen, J., May, S.M., Brückner, H., 2016. Tsunami deposits of the Caribbean – Towards an
809 improved coastal hazard assessment. Earth-Science Reviews 163, 260–296.
810 https://doi.org/10.1016/j.earscirev.2016.10.010
811 Feuillet, N., Beauducel, F., Jacques, E., Tapponnier, P., Delouis, B., Bazin, S., Vallée, M., King, G.C.P.,
812 2011. The Mw = 6.3, November 21, 2004, Les Saintes earthquake (Guadeloupe): Tectonic

setting, slip model and static stress changes. Journal of Geophysical Research 116. https://doi.org/10.1029/2011JB008310

Feuillet, N., Beauducel, F., Tapponnier, P., 2011. Tectonic context of moderate to large historical earthquakes in the Lesser Antilles and mechanical coupling with volcanoes. Journal of Geophysical Research 116. https://doi.org/10.1029/2011JB008443

Fuentes, Z., Tuttle, M.P., Schmidt, W.E., 2017. Sand Scripts of Past Tsunamis in Coastal Ponds of St. Thomas, U.S. Virgin Islands. Seismological Research Letters 88, 1516–1526. https://doi.org/10.1785/0220170038

Garnier, E., Desarthe, J., Moncoulon, D., 2015. The historic reality of the cyclonic variability in French Antilles, 1635–2007. Climate of the Past Discussions 11, 1519–1550. https://doi.org/10.5194/cpd-11-1519-2015

Goff, J., McFadgen, B.G., Chagué-Goff, C., 2004. Sedimentary differences between the 2002 Easter storm and the 15th-century Okoropunga tsunami, southeastern North Island, New Zealand. Marine Geology 204, 235–250. https://doi.org/10.1016/S0025-3227(03)00352-9

Goldberg, E. G, 1963. Geochronology with 210Pb. Radioactive Dating, International Atomic Energy Agency, Vienna, 121–131.

Goto, K., Miyagi, K., Imamura, F., 2013. Localized tsunamigenic earthquakes inferred from preferential distribution of coastal boulders on the Ryukyu Islands, Japan. Geology 41, 1139–1142. https://doi.org/10.1130/G34823.1

Hallock, P., Glenn, E.C., 1986. Larger Foraminifera: A Tool for Paleoenvironmental Analysis of Cenozoic Carbonate Depositional Facies. PALAIOS 1, 55. https://doi.org/10.2307/3514459

Harbitz, C.B., Glimsdal, S., Bazin, S., Zamora, N., Løvholt, F., Bungum, H., Smebye, H., Gauer, P., Kjekstad, O., 2012. Tsunami hazard in the Caribbean: Regional exposure derived from credible worst case scenarios. Continental Shelf Research 38, 1–23. https://doi.org/10.1016/j.csr.2012.02.006

Heiri, O., Lotter, A.F., Lemcke, G., n.d. Loss on ignition as a method for estimating organic and carbonate content in sediments: reproducibility and comparability of results 10.

840 Hoggarth, D., 2001. Management Plan for the Marine Parks of Anguilla. Prepared for: Organisation of
841 Eastern Caribbean States Natural Resources Management Unit St Lucia. Department for
842 International Development 65.
843 Hough, S.E., 2013. Missing great earthquakes. Journal of Geophysical Research: Solid Earth 118, 1098–
844 1108. https://doi.org/10.1002/jgrb.50083
845 Jaffe, B.E., Gelfenbaum, G., Rubin, D.M., Peters, R., Anima, R., Swensson, M., Olcese, D., Anticona,
846 L.B., Gomez, J.C., Riega, P.C., 2003. Identification and interpretation of tsunami deposits from
847 the June 23, 2001 Peru tsunami 12.
848 Jankaew, K., Atwater, B.F., Sawai, Y., Choowong, M., Charoentitirat, T., Martin, M.E., Prendergast,
849 A., 2008. Medieval forewarning of the 2004 Indian Ocean tsunami in Thailand. Nature 455,
850 1228–1231. https://doi.org/10.1038/nature07373
851 Jury, M., Malmgren, B.A., Winter, A., 2007. Subregional precipitation climate of the Caribbean and
852 relationships with ENSO and NAO. Journal of Geophysical Research 112.
853 https://doi.org/10.1029/2006JD007541
854 Kanaya, G., Maki, H., Suzuki, T., Sato-Okoshi, W., Kikuchi, E., 2015. Tsunami-induced Changes in a
855 Shallow Brackish Lagoon Ecosystem (Gamo Lagoon) in Sendai Bay, Japan 12.
856 Khan, N.S., Ashe, E., Horton, B.P., Dutton, A., Kopp, R.E., Brocard, G., Engelhart, S.E., Hill, D.F.,
857 Peltier, W.R., Vane, C.H., Scatena, F.N., 2017. Drivers of Holocene sea-level change in the
858 Caribbean. Quaternary Science Reviews 155, 13–36.
859 https://doi.org/10.1016/j.quascirev.2016.08.032
860 Kusumoto, S., Goto, T., Sugai, T., Omori, T., Satake, K., 2018. Geological evidence of tsunamis in the
861 past 3800 years at a coastal lowland in the Central Fukushima Prefecture, Japan. Marine
862 Geology 404, 137–146. https://doi.org/10.1016/j.margeo.2018.07.004
863 Lander, J.F., Whiteside, L.S., Lockridge, P.A., 2002. A brief history of tsunamis in the Caribbean Sea.
864 Science of Tsunami Hazards 20, 57.
865 Le Friant, A., Heinrich, P., Boudon, G., 2008. Field survey and numerical simulation of the 21
866 November 2004 tsunami at Les Saintes (Lesser Antilles): tsunami at Les Saintes, 21 November
867 2004. Geophysical Research Letters 35, n/a-n/a. https://doi.org/10.1029/2008GL034051

Liu, K., Fearn, M.L., 2000. Reconstruction of Prehistoric Landfall Frequencies of Catastrophic Hurricanes in Northwestern Florida from Lake Sediment Records. Quaternary Research 54, 238–245. https://doi.org/10.1006/qres.2000.2166

Liu, K., Fearn, M.L., 1993. Lake-sediment record of late Holocene hurricane activities from coastal Alabama. Geology 21, 793–796.

Malaizé, B., Bertran, P., Carbonel, P., Bonnissent, D., Charlier, K., Galop, D., Imbert, D., Serrand, N., Stouvenot, Ch., Pujol, C., 2011. Hurricanes and climate in the Caribbean during the past 3700 years BP. The Holocene 21, 911–924. https://doi.org/10.1177/0959683611400198

McCloskey, T.A., Keller, G., 2009. 5000 year sedimentary record of hurricane strikes on the central coast of Belize. Quaternary International 195, 53–68. https://doi.org/10.1016/j.quaint.2008.03.003

Morton, R.A., Clifton, H.E., Buster, N.A., Peterson, R.L., Gelfenbaum, G., 2007a. Forcing of large-scale cycles of coastal change at the entrance to Willapa Bay, Washington. Marine Geology 246, 24–41. https://doi.org/10.1016/j.margeo.2007.07.008

Morton, R.A., Gelfenbaum, G., Jaffe, B.E., 2007b. Physical criteria for distinguishing sandy tsunami and storm deposits using modern examples. Sedimentary Geology 200, 184–207. https://doi.org/10.1016/j.sedgeo.2007.01.003

Morton, R.A., Gelfenbaum, G., Jaffe, B.E., 2007c. Physical criteria for distinguishing sandy tsunami and storm deposits using modern examples. Sedimentary Geology 200, 184–207. https://doi.org/10.1016/j.sedgeo.2007.01.003

Muhs, D.R., Budahn, J.R., 2009. Geochemical evidence for African dust and volcanic ash inputs to terra rossa soils on carbonate reef terraces, northern Jamaica, West Indies. Quaternary International 196, 13–35. https://doi.org/10.1016/j.quaint.2007.10.026

Muhs, D.R., Budahn, J.R., Prospero, J.M., Carey, S.N., 2007. Geochemical evidence for African dust inputs to soils of western Atlantic islands: Barbados, the Bahamas, and Florida. Journal of Geophysical Research 112. https://doi.org/10.1029/2005JF000445

Muhs, D.R., Budahn, J.R., Prospero, J.M., Skipp, G., Herwitz, S.R., 2012. Soil genesis on the island of Bermuda in the Quaternary: The importance of African dust transport and deposition: African

dust in Bermuda soils. Journal of Geophysical Research: Earth Surface 117, n/a-n/a. https://doi.org/10.1029/2012JF002366

Munger, S., Cheung, K.F., 2008. Resonance in Hawaii waters from the 2006 Kuril Islands Tsunami: the 2006 Kuril Islands tsunami. Geophysical Research Letters 35, n/a-n/a. https://doi.org/10.1029/2007GL032843

Murakami, H., Levin, E., Delworth, T.L., Gudgel, R., Hsu, P.-C., 2018. Dominant effect of relative tropical Atlantic warming on major hurricane occurrence. Science 362, 794–799. https://doi.org/10.1126/science.aat6711

Murray, J.W., 2006. Ecology and Applications of Benthic Foraminifera.

Nanayama, F., Satake, K., Furukawa, R., Shimokawa, K., Atwater, B.F., Shigeno, K., Yamaki, S., 2003. Unusually large earthquakes inferred from tsunami deposits along the Kuril trench. Nature 424, 660–663. https://doi.org/10.1038/nature01864

Nanayama, F., Shigeno, K., Satake, K., Shimokawa, K., Koitabashi, S., Miyasaka, S., Ishii, M., 2000. Sedimentary differences between the 1993 Hokkaido-nansei-oki tsunami and the 1959 Miyakojima typhoon at Taisei, southwestern Hokkaido, northern Japan. Sedimentary Geology 135, 255–264. https://doi.org/10.1016/S0037-0738(00)00076-2

Naruse, H., Fujino, S., Suphawajruksakul, A., Jarupongsakul, T., 2010. Features and formation processes of multiple deposition layers from the 2004 Indian Ocean Tsunami at Ban Nam Kem, southern Thailand: Multiple deposition layers from tsunami. Island Arc 19, 399–411. https://doi.org/10.1111/j.1440-1738.2010.00732.x

Oliva, F., Viau, A.E., Peros, M.C., Bouchard, M., 2018. Paleotempestology database for the western North Atlantic basin. The Holocene 28, 1664–1671. https://doi.org/10.1177/0959683618782598

Pelinovsky, E., Zahibo, N., Dunkley, P., Edmonds, M., Herd, R., Talipova, T., Kozelkov, A., Nikolkina, I., 2004. Tsunami Generated By the Volcano Eruption On July 12-13, 2003 At Montserrat, Lesser Antilles. Science of Tsunami Hazards 22, 15.

Pennington, W., Tutin, T.G., Cambray, R.S., Fisher, E.M., 1973. Observations on Lake Sediments using Fallout 137Cs as a Tracer. Nature 242, 324–326. https://doi.org/10.1038/242324a0

924 Pilarczyk, J.E., Horton, B.P., Soria, J.L.A., Switzer, A.D., Siringan, F., Fritz, H.M., Khan, N.S.,
925 Ildefonso, S., Doctor, A.A., Garcia, M.L., 2016. Micropaleontology of the 2013 Typhoon
926 Haiyan overwash sediments from the Leyte Gulf, Philippines. Sedimentary Geology 339, 104–
927 114. https://doi.org/10.1016/j.sedgeo.2016.04.001
928 Pinet, C., 2011. New aerial survey of Anguilla, European R3 Regional Risk Reduction initiative- United
929 Nations Development Program, contract BAR/UNDP/PSC/2011/003, IGN/IMAO report for the
930 Government of Anguilla.
931 Prospero, J.M., 2003. African Droughts and Dust Transport to the Caribbean: Climate Change
932 Implications. Science 302, 1024–1027. https://doi.org/10.1126/science.1089915
933 R Core Team, 2014. R: A language and environment for statistical computing. R Foundation for
934 Statistical Computing, Vienna, Austria.
935 Reguero, M., Raz-Guzmán, A., 2018. Molluscs (Mollusca: Gastropoda, Bivalvia, Polyplacophora) of
936 Laguna Madre, Tamaulipas, Mexico: Spatial and Temporal Distribution. Gulf of Mexico
937 Science 34, 32–55. https://doi.org/10.18785/goms.3401.04
938 Reid, H.F., Taber, S., 1920. The Virgin Islands earthquakes of 1867-1868. Bull. Seismol. Soc. Am. 10,
939 9–30.
940 Reimer, P.J., Bard, E., Bayliss, A., Beck, J.W., Blackwell, P.G., Ramsey, C.B., Buck, C.E., Cheng, H.,
941 Edwards, R.L., Friedrich, M., Grootes, P.M., Guilderson, T.P., Haflidason, H., Hajdas, I., Hatté,
942 C., Heaton, T.J., Hoffmann, D.L., Hogg, A.G., Hughen, K.A., Kaiser, K.F., Kromer, B.,
943 Manning, S.W., Niu, M., Reimer, R.W., Richards, D.A., Scott, E.M., Southon, J.R., Staff, R.A.,
944 Turney, C.S.M., van der Plicht, J., 2013. IntCal13 and Marine13 Radiocarbon Age Calibration
945 Curves 0–50,000 Years cal BP. Radiocarbon 55, 1869–1887.
946 https://doi.org/10.2458/azu_js_rc.55.16947
947 Reyss, J.-L., Schmidt, S., Legeleux, F., Bonté, P., 1995. Large, low background well-type detectors for
948 measurements of environmental radioactivity. Nuclear Instruments and Methods in Physics
949 Research Section A: Accelerators, Spectrometers, Detectors and Associated Equipment 357,
950 391–397. https://doi.org/10.1016/0168-9002(95)00021-6

951 Ribeiro Guevara, S., Rizzo, A., Daga, R., Williams, N., Villa, S., 2019. Bromine as indicator of source
952 of lacustrine sedimentary organic matter in paleolimnological studies. Quaternary Research 92,
953 257–271. https://doi.org/10.1017/qua.2018.125
954 Richter, T.O., van der Gaast, S., Koster, B., Vaars, A., Gieles, R., de Stigter, H.C., De Haas, H., van
955 Weering, T.C.E., 2006. The Avaatech XRF Core Scanner: technical description and applications
956 to NE Atlantic sediments. Geological Society, London, Special Publications 267, 39–50.
957 https://doi.org/10.1144/GSL.SP.2006.267.01.03
958 Riou, B., Chaumillon, E., Schneider, J., Corrège, T., Chagué, C., 2019. The sediment-fill of Pago Pago
959 Bay (Tutuila Island, American Samoa): New insights on the sediment record of past tsunamis.
960 Sedimentology. https://doi.org/10.1111/sed.12574
961 Roger, J., Baptista, M.A., Sahal, A., Accary, F., Allgeyer, S., Hébert, H., 2011. The Transoceanic 1755
962 Lisbon Tsunami in Martinique. Pure and Applied Geophysics 168, 1015–1031.
963 https://doi.org/10.1007/s00024-010-0216-8
964 Sabatier, P., Dezileau, L., Briqueu, L., Colin, C., Siani, G., 2010. Clay minerals and geochemistry record
965 from northwest Mediterranean coastal lagoon sequence: Implications for paleostorm
966 reconstruction. Sedimentary Geology 228, 205–217.
967 https://doi.org/10.1016/j.sedgeo.2010.04.012
968 Sabatier, P., Dezileau, L., Colin, C., Briqueu, L., Bouchette, F., Martinez, P., Siani, G., Raynal, O., Von
969 Grafenstein, U., 2012. 7000 years of paleostorm activity in the NW Mediterranean Sea in
970 response to Holocene climate events. Quaternary Research 77, 1–11.
971 https://doi.org/10.1016/j.yqres.2011.09.002
972 Sabatier, P., Dezileau, L., Condomines, M., Briqueu, L., Colin, C., Bouchette, F., Le Duff, M.,
973 Blanchemanche, P., 2008. Reconstruction of paleostorm events in a coastal lagoon (Hérault,
974 South of France). Marine Geology 251, 224–232. https://doi.org/10.1016/j.margeo.2008.03.001
975 Sabatier, P., Wilhelm, B., Ficetola, G.F., Moiroux, F., Poulenard, J., Develle, A.-L., Bichet, A., Chen,
976 W., Pignol, C., Reyss, J.-L., Gielly, L., Bajard, M., Perrette, Y., Malet, E., Taberlet, P., Arnaud,
977 F., 2017. 6-kyr record of flood frequency and intensity in the western Mediterranean Alps –

978 Interplay of solar and temperature forcing. Quaternary Science Reviews 170, 121–135.
979 https://doi.org/10.1016/j.quascirev.2017.06.019
980 Sainte-Claire Deville, C., 1843. Observations sur le tremblement de terre éprouvé à la Guadeloupe le 8
981 Février 1843. Imprimerie du Gouverneur, Basse-Terre.
982 Scheffers, A., Scheffers, S., Kelletat, D., 2005. Paleo-Tsunami Relics on the Southern and Central
983 Antillean Island Arc. Journal of Coastal Research 212, 263–273. https://doi.org/10.2112/03-
984 0144.1
985 Scheucher, L.E.A., Vortisch, W., 2011. Field survey and hydrodynamics of storm-deposited boulders in
986 the southwestern Dominican Republic: Playa Azul, Provincia De Barahona. Bornemann, A.,
987 Brachert, T.C., Ehrmann, W. (Eds.), SEDIMENT 2011 – Sediments: Archives of the Earth
988 System, Leipzig, June 23–26, 2011 88–89.
989 Schindelin, J., Arganda-Carreras, I., Frise, E., Kaynig, V., Longair, M., Pietzsch, T., Preibisch, S.,
990 Rueden, C., Saalfeld, S., Schmid, B., Tinevez, J.-Y., White, D.J., Hartenstein, V., Eliceiri, K.,
991 Tomancak, P., Cardona, A., 2012. Fiji: an open-source platform for biological-image analysis.
992 Nature Methods 9, 676–682. https://doi.org/10.1038/nmeth.2019
993 Scileppi, E., Donnelly, J.P., 2007. Sedimentary evidence of hurricane strikes in western Long Island,
994 New York: hurricane strikes in New York. Geochemistry, Geophysics, Geosystems 8, n/a-n/a.
995 https://doi.org/10.1029/2006GC001463
996 Shepherd, J.B., 1992. Comment on “subduction and seismic hazard in the Lesser Antilles” by Pascal
997 Bernard and Jerome Lambert 10.
998 Shinozaki, T., Goto, K., Fujino, S., Sugawara, D., Chiba, T., 2015. Erosion of a paleo-tsunami record
999 by the 2011 Tohoku-oki tsunami along the southern Sendai Plain. Marine Geology 369, 127–
1000 136. https://doi.org/10.1016/j.margeo.2015.08.009
1001 Uchida, J.-I., Fujiwara, O., Hasegawa, S., Kamataki, T., 2010. Sources and depositional processes of
1002 tsunami deposits: Analysis using foraminiferal tests and hydrodynamic verification: Sources of
1003 tsunami deposits. Island Arc 19, 427–442. https://doi.org/10.1111/j.1440-1738.2010.00733.x
1004 Van der Does, M., Korte, L.F., Munday, C.I., Brummer, G.-J.A., Stuut, J.-B.W., 2016. Particle size
1005 traces modern Saharan dust transport and deposition across the equatorial North Atlantic.

1006 Atmospheric Chemistry and Physics 16, 13697–13710. https://doi.org/10.5194/acp-16-13697-
1007 2016
1008 Wallace, E.J., Donnelly, J.P., Hengstum, P.J., Wiman, C., Sullivan, R.M., Winkler, T.S., d'Entremont,
1009 N.E., Toomey, M., Albury, N., 2019. Intense Hurricane Activity Over the Past 1500 Years at
1010 South Andros Island, The Bahamas. Paleoceanography and Paleoclimatology 34, 1761–1783.
1011 https://doi.org/10.1029/2019PA003665
1012 Ward (nee Milne), J.M., 1967. Studies in ecology on a shell barrier beach section III chemical factors
1013 of the environment. Vegetatio Acta Geobotanica 15, 77–112.
1014 https://doi.org/10.1007/BF01959618
1015 Watt, S.F.L., Talling, P.J., Vardy, M.E., Heller, V., Hühnerbach, V., Urlaub, M., Sarkar, S., Masson,
1016 D.G., Henstock, T.J., Minshull, T.A., Paulatto, M., Le Friant, A., Lebas, E., Berndt, C.,
1017 Crutchley, G.J., Karstens, J., Stinton, A.J., Maeno, F., 2012. Combinations of volcanic-flank
1018 and seafloor-sediment failure offshore Montserrat, and their implications for tsunami
1019 generation. Earth and Planetary Science Letters 319–320, 228–240.
1020 https://doi.org/10.1016/j.epsl.2011.11.032
1021 Wedepohl, K.H., 1971. Environmental influences on the chemical composition of shales and clays.
1022 Physics and Chemistry of the Earth 8, 307–333. https://doi.org/10.1016/0079-1946(71)90020-
1023 6
1024 Weiss, M.P., 1979. A Saline Lagoon on Cayo Sal, Western Venezuela. Atoll Research Bulletin 1–25.
1025 https://doi.org/10.5479/si.00775630.232.1
1026 Woodruff, J.D., Donnelly, J.P., Okusu, A., 2009. Exploring typhoon variability over the mid-to-late
1027 Holocene: evidence of extreme coastal flooding from Kamikoshiki, Japan. Quaternary Science
1028 Reviews 28, 1774–1785. https://doi.org/10.1016/j.quascirev.2009.02.005
1029 Zahibo, N., Pelinovsky, E., Okal, E., Yalçiner, A., Kharif, C., Talipova, T., Kozelkov, A., 2005. The
1030 earthquake and tsunami of November 21, 2004 at Les Saintes, Guadeloupe, Lesser Antilles.
1031 Science of Tsunami Hazards 23, 25.

1032 Zahibo, N., Pelinovsky, E., Yalciner, A.C., Kurkin, A., Koselkov, A., Zaitsev, A., 2003. The 1867 Virgin
1033 Island Tsunami. Natural Hazards and Earth System Sciences 3, 367–376.
1034 https://doi.org/10.5194/nhess-3-367-2003
1035 Zahibo, N., Pelinovsky, E.N., 2001. Evaluation of tsunami risk in the Lesser Antilles. Natural Hazards
1036 and Earth System Sciences 1, 221–231. https://doi.org/10.5194/nhess-1-221-2001
1037

Figures and Tables

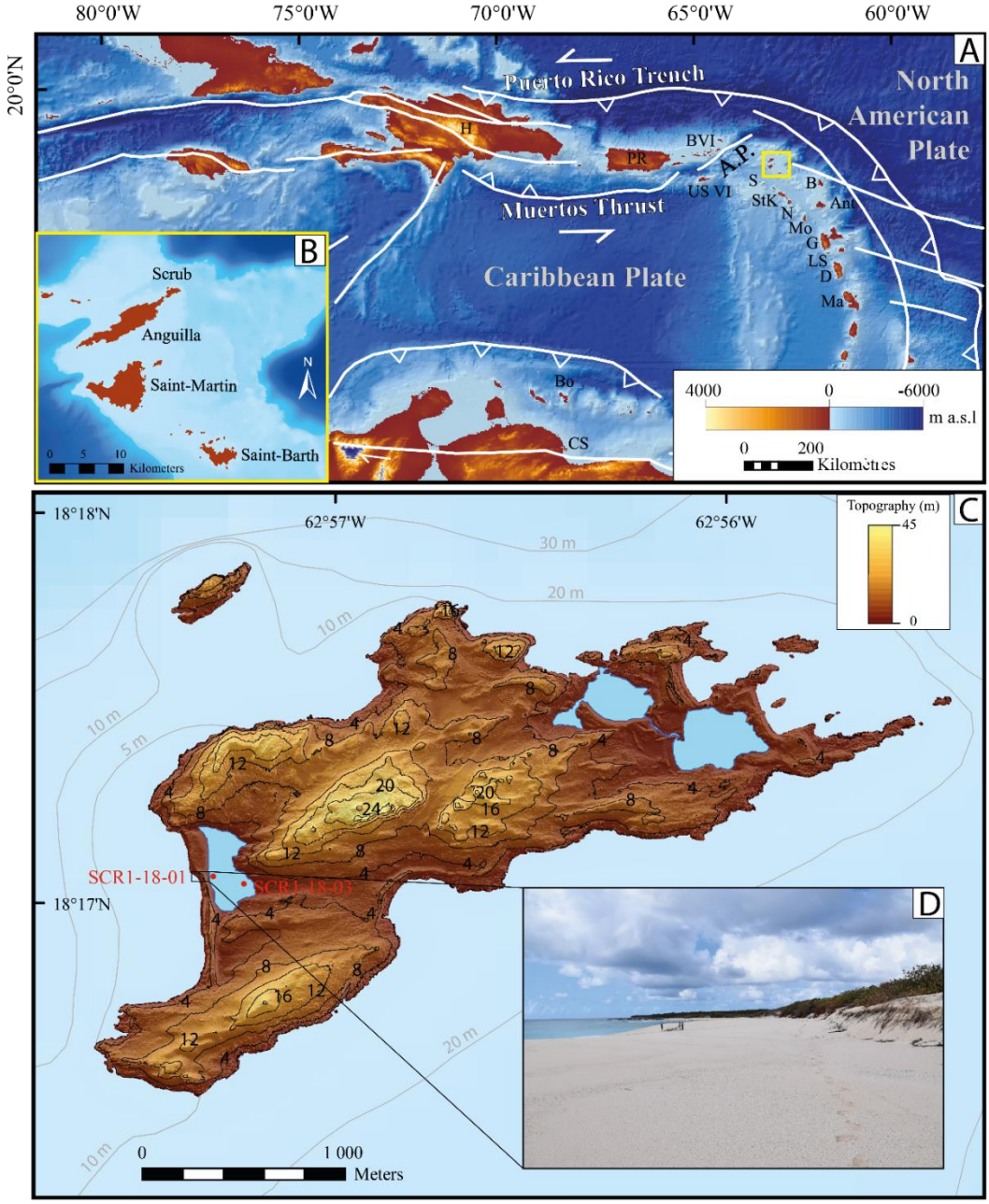

Figure 1. A: The Caribbean Sea with main faults (A.P.: Anegada Passage) and islands (H: Hispaniola, PR: Puerto Rico, BVI: British Virgin Islands, US VI: US Virgin Islands, S: Saba, StK: Saint-Kitts, N: Nevis, B: Barbuda, Ant: Antigua, Mo: Montserrat, G: Guadeloupe, LS: Les Saintes, D: Dominique, Ma: Martinique), modified from Feuillet et al. (2002, 2011 and references therein). The bathymetry and topographic DEM (Digital Elevation model) are derived from the SHOM (Service hydrographique et océanographique de la Marine) website (SHOM, 2018). The small yellow square corresponds to the Anguilla-Saint-Barthelemy platform shown in Fig. 1B. **B**: The Anguilla-Saint-Barthelemy platform with

its islands. **C**: Scrub Island. The topographic data were obtained by LIDAR (Pinet, 2011) and the bathymetric isolines were digitalized from the marine map on the SHOM website (data.shom.fr/donnees/legend/RASTER_MARINE_3857_WMTS). The 2 red dots indicate the location of the sediment cores. **D**: Sandy barrier of Scrub Island, March 2018 (photo by E. Chaumillon).

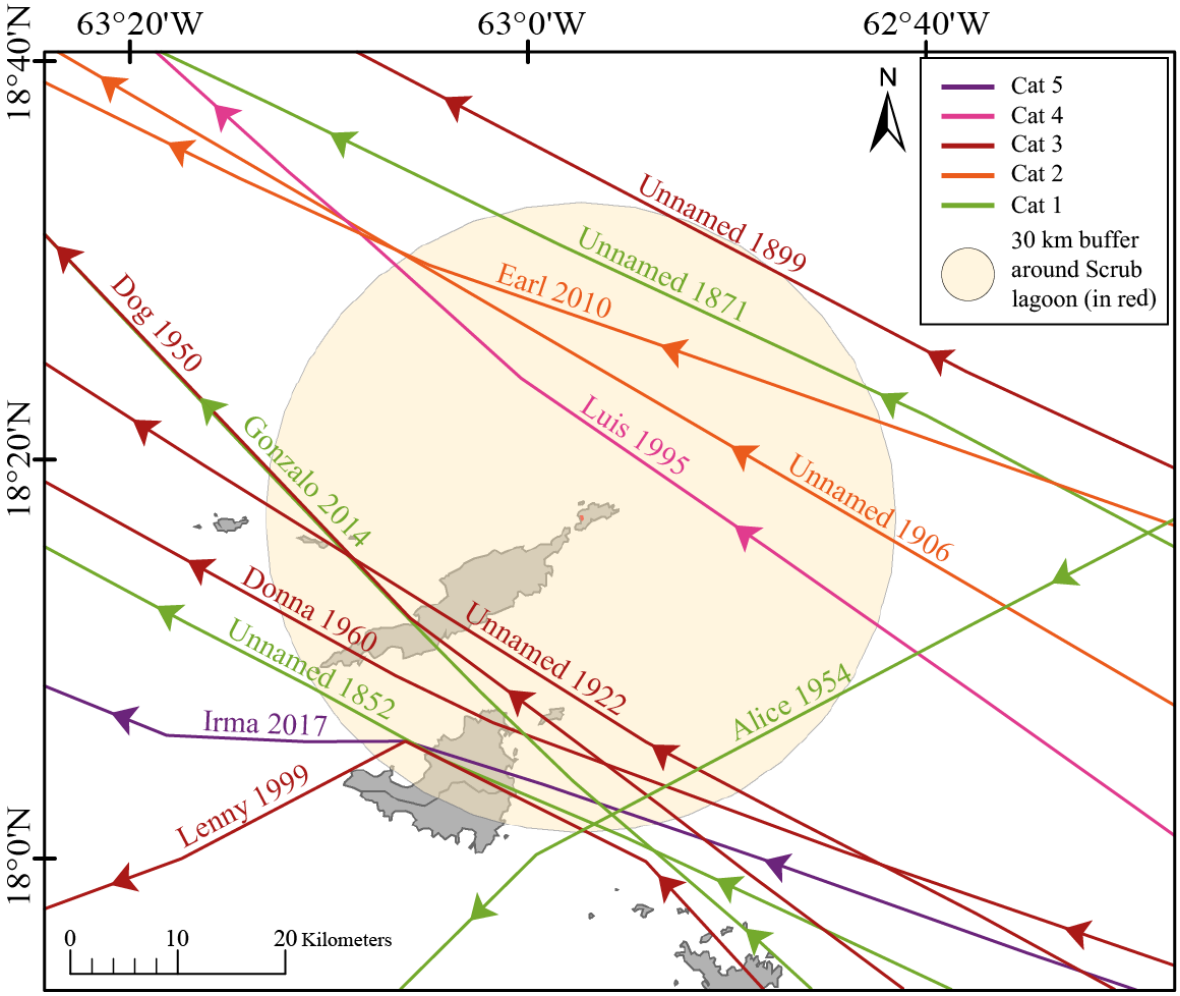

Figure 2. Historical hurricane tracks (1852–2017) passing within 30 km of the westernmost Scrub Island lagoon (coast.noaa.gov/hurricanes, 2020).

Year	Name	Month	Hurricane category (SSHWS) within 30 km around Scrub	Distance hurricane-Scrub (km)	Hurricane path with respect to Anguilla Island	Wind speed (kt)	Pressure (mb)
2017	Irma	September	H5	25	SW	155	914
2014	Gonzalo	October	H1	18	NW	74	984
2010	Earl	September	H2	18	NE	95	967
1999	Lenny	November	H2	26	SW	85	975
1995	Luis	September	H4	8	NE	115	942
1960	Donna	September	H3	21	NW	110	952
1955	Alice	January	H1	26	SE	65	991
1950	Dog	September	H3	17	NW	105	NA
1922	Unnamed	September	H3	15	NW	100	NA
1906	Unnamed	September	H2	13	NE	90	NA
1899	Unnamed	September	H3	29	NE	100	NA
1871	Unnamed	September	H1	23	NE	75	NA
1852	Unnamed	September	H1	26	NW	70	NA

Table 1. Hurricanes that passed within 30 km from Scrub Island (Anguilla) from 1852 to 2017 (coast.noaa.gov/hurricanes, 2020). SSHWS: Saffir–Simpson hurricane wind scale. Kt = knot, mb = millibar.

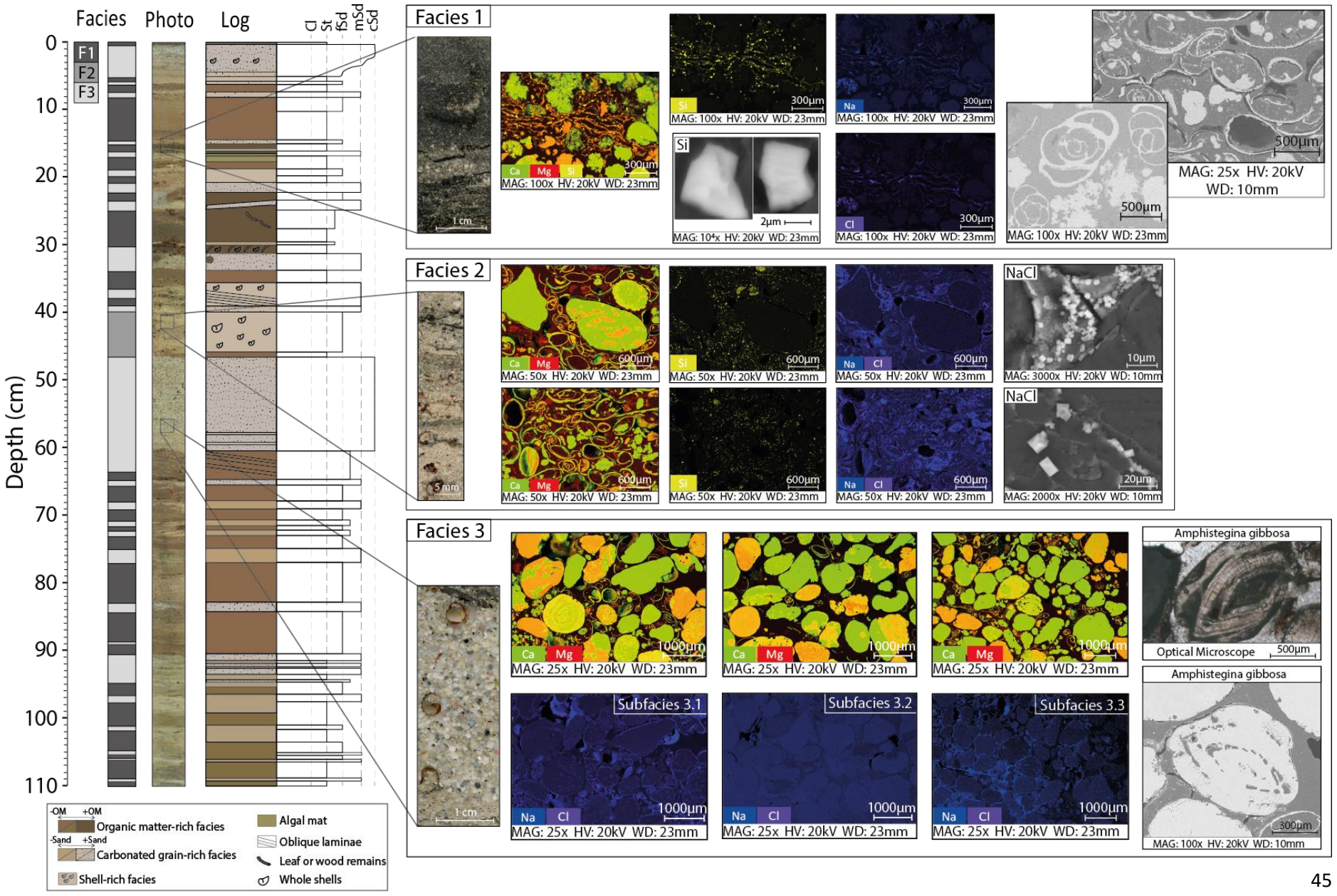
Facies
Photo
Log
Cl
St
fSd
mSd
cSd
F1
F2
F3
Depth (cm)
0
10
20
30
40
50
60
70
80
90
100
110
Facies 1
1 cm
Ca Mg Si
MAG: 100x HV: 20kV WD: 23mm
Si
MAG: 100x HV: 20kV WD: 23mm
Na
MAG: 100x HV: 20kV WD: 23mm
2µm
MAG: 10⁴x HV: 20kV WD: 23mm
Cl
MAG: 100x HV: 20kV WD: 23mm
500µm
MAG: 100x HV: 20kV WD: 23mm
MAG: 25x HV: 20kV
WD: 10mm
Facies 2
5 mm
Ca Mg
MAG: 50x HV: 20kV WD: 23mm
Si
MAG: 50x HV: 20kV WD: 23mm
Na Cl
MAG: 50x HV: 20kV WD: 23mm
NaCl
MAG: 3000x HV: 20kV WD: 10mm
NaCl
MAG: 2000x HV: 20kV WD: 10mm
Facies 3
1 cm
MAG: 25x HV: 20kV WD: 23mm
Subfacies 3.1
Subfacies 3.2
Subfacies 3.3
Amphistegina gibbosa
Optical Microscope
Amphistegina gibbosa
MAG: 100x HV: 20kV WD: 10mm
-OM +OM
Organic matter-rich facies
-Sand +Sand
Carbonated grain-rich facies
Shell-rich facies
Algal mat
Oblique laminae
Leaf or wood remains
Whole shells

Figure 3. Facies of core SCR1-18-01. On the left of the figure: Facies, photo and sedimentary log. On the right of the image: the three main facies of the core. For every facies there is: a picture of a thin slide on the left, SEM images, geochemical cartographies (with Ca in green, Mg in red, Si in yellow, Na in blue and Cl in purple). On the top right corner of Facies 3, there is a photograph of a foraminifera (Amphistegina gibbosa) taken from an optical microscope.

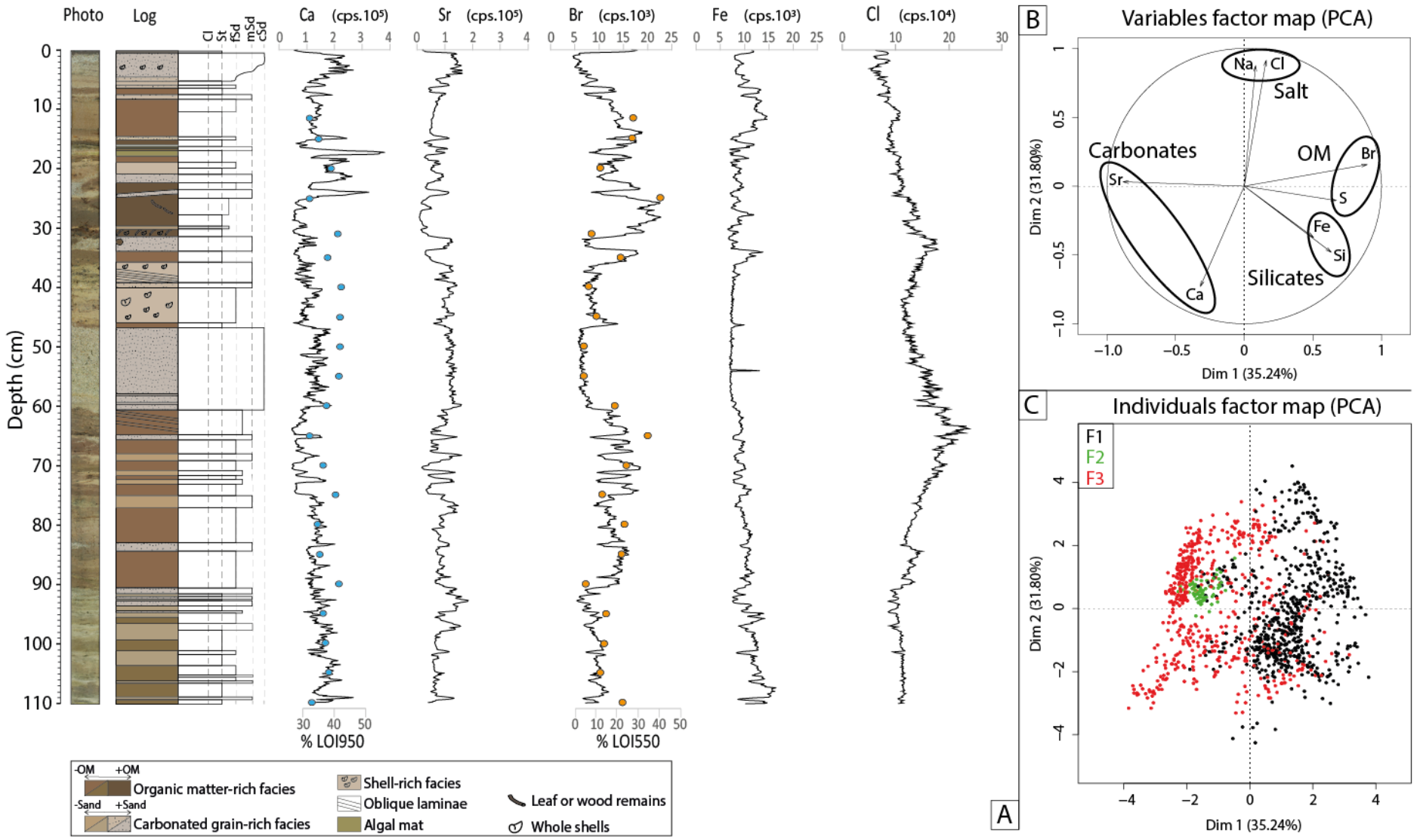
Photo
Log
Cl
St
fSd
mSd
cSd
Ca (cps.10⁵)
Sr (cps.10⁵)
Br (cps.10³)
Fe (cps.10³)
Cl (cps.10⁴)
Depth (cm)
% LOI950
% LOI550
-OM
+OM
Organic matter-rich facies
-Sand
+Sand
Carbonated grain-rich facies
Shell-rich facies
Oblique laminae
Algal mat
Leaf or wood remains
Whole shells
B
Variables factor map (PCA)
Na
Cl
Salt
Carbonates
OM
Br
Sr
S
Fe
Si
Silicates
Ca
Dim 1 (35.24%)
Dim 2 (31.80%)
C
Individuals factor map (PCA)
F1
F2
F3
A

Figure 4. Geochemical data for core SCR1-18-01. A: From left to right, picture, sedimentary log, XRF data for Ca, Sr, Br, Fe and Cl. The LOI950 and LOI550 percentages from the LOI analyses are superposed on the Ca and Br XRF data, respectively. B: PCA analyses from the XRF data. C: Map of the geochemical data distribution with the facies information. The black dots correspond to Facies 1, the green dots to Facies 2 and the red dots to Facies 3.

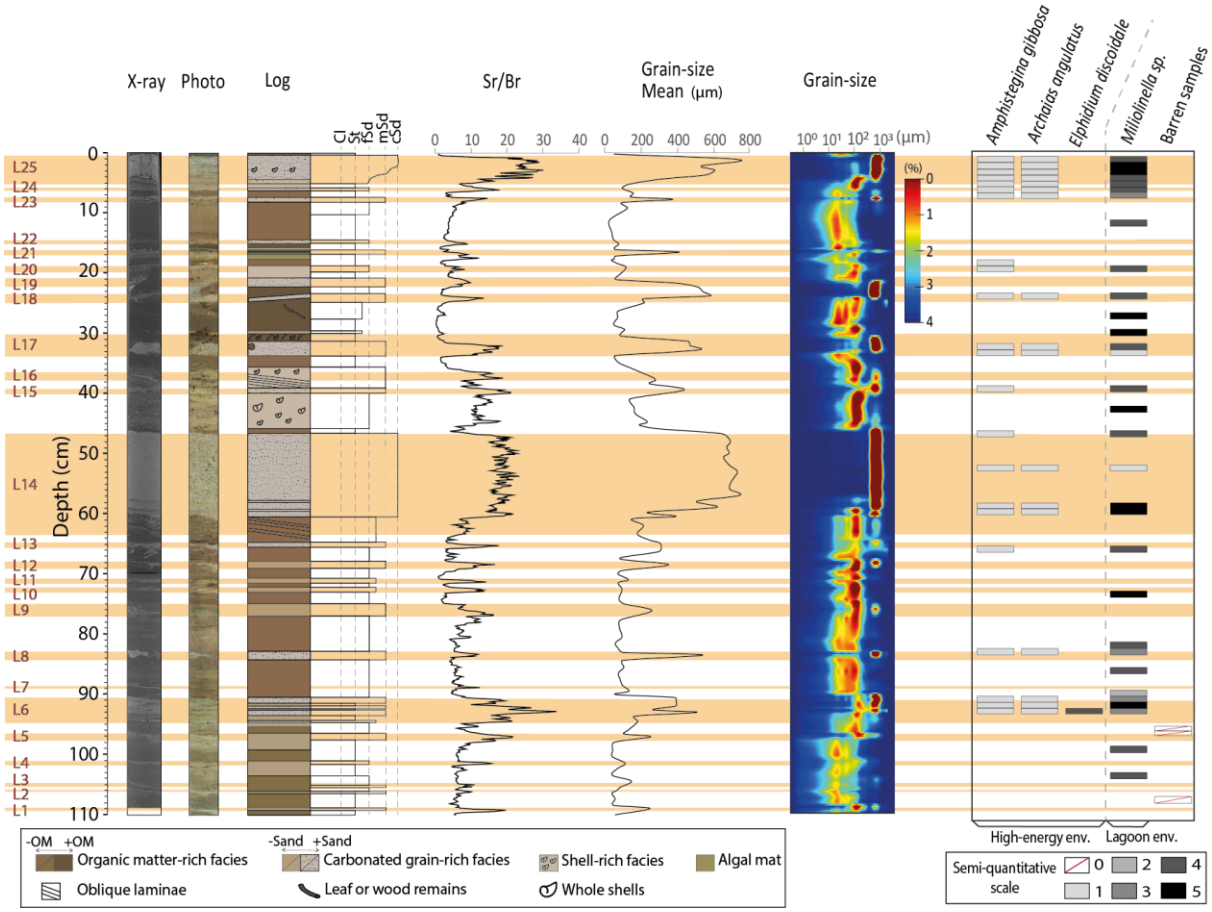

Figure 5. Data for core SCR1-18-01. From left to right: F3 Layers (in red) associated to the orange lines, X-ray, photograph, sedimentary log, ratio Sr/Br from the XRF data, mean grain-size, map of the grain size distribution, Abundance of High-energy environment and lagoon environment foraminifera (125-500 µm and >500 µm fractions) according to a semi-quantitative scale: 0= no individuals, 1= 1 to 2 individuals, 2= 3 to 5 individuals, 3= 6 to 15 individuals, 4= 16 to 40 individuals, 5= more than 41 individuals.

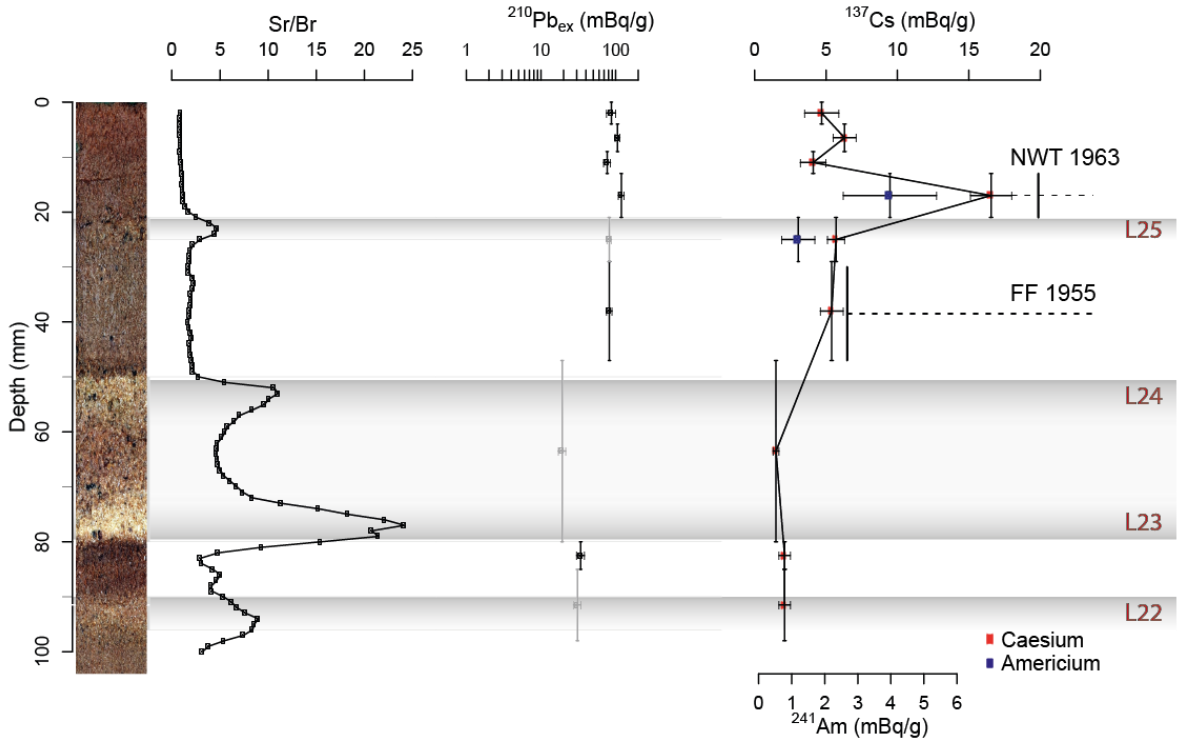

Figure 6. SCR1-18-03 short-lived radionuclide data with the excess 210Pb in logarithmic scale associated with the 137Cs (NWT: Nuclear Weapon Tests; FF: First Fallout recorded) and 241Am profiles and Sr/Br XRF ratio.

Sample Name	Core	Depth (cm)	Sample type	Age (AD /BC)	Calibrated age ranges at 95% confidence interval (cal. AD /BC)
Poz-111671	SCR1-18-01	14.5	Plant macroremains	1805 ± 30	1668-1947
SacA54690	SCR1-18-01	21	Plant macroremains	1795 ± 30	1666-1950
SacA54691	SCR1-18-01	31	Plant macroremains	1725 ± 30	1641-1950
Poz-111673	SCR1-18-01	43.5	Plant macroremains	1590 ± 30	1452-1634
Poz-111674	SCR1-18-01	64	Plant macroremains	1285 ± 30	1276-1391
SacA54692	SCR1-18-01	71.5	Plant macroremains	1005 ± 30	1026-1155
Poz-111675	SCR1-18-01	80	Plant macroremains	825 ± 30	778-990
Poz-111677	SCR1-18-01	89.5	Plant macroremains	755 ± 30	721-941
Poz-111678	SCR1-18-01	96	Plant macroremains	635 ± 30	655-768
SacA54693	SCR1-18-01	105	Plant macroremains	335 ± 30	389-536
Poz-111679	SCR1-18-03	44.5	Plant macroremains	775 ± 30	770-962
Poz-111680	SCR1-18-03	64.5	Plant macroremains	105 ± 30	86-238
Poz-111681	SCR1-18-03	98.5	Plant macroremains	980 BC ± 30	1132 BC-1027 BC

Table 2. 14C ages for cores SCR1-18-01 and SCR1-18-03 (plant macroremains: wood or leaves).

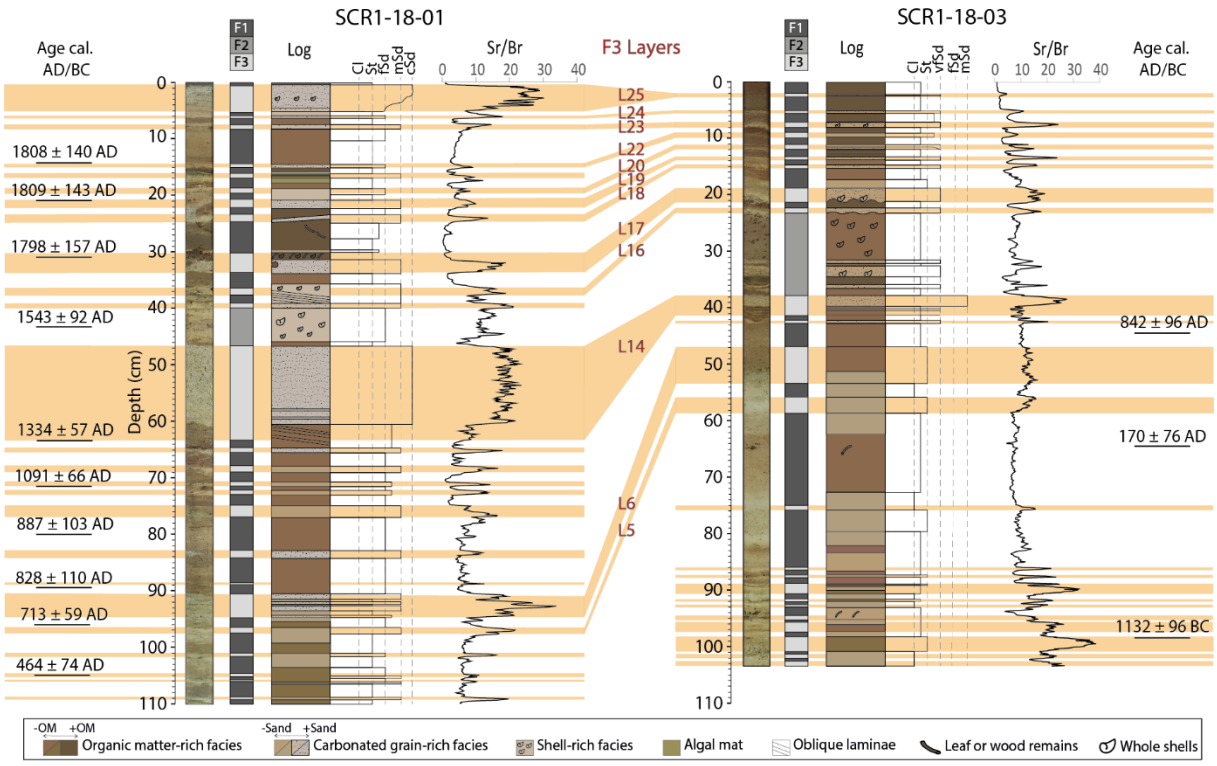

Figure 7. Sedimentary logs for cores SCR1-18-01 and SCR1-18-03 with the depth of the 14C ages in cal. AD/BC. The orange lines highlight the F3 layers from both cores that were correlated.

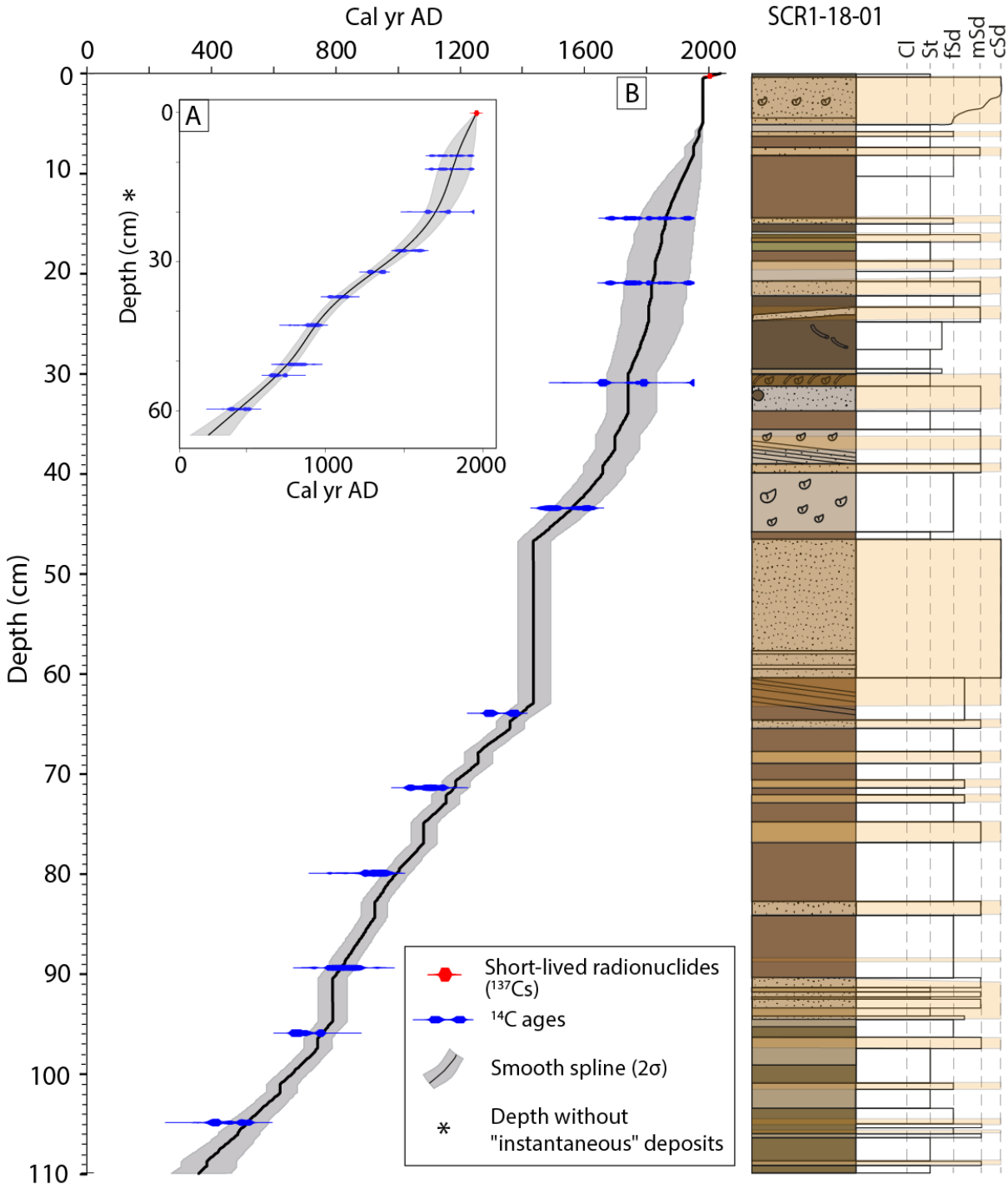

Figure 8. Age model. A: Age-depth model with instantaneous-event-free depth. B: Age-depth model from radiocarbon ages and short-lived radionuclides data (137Cs).

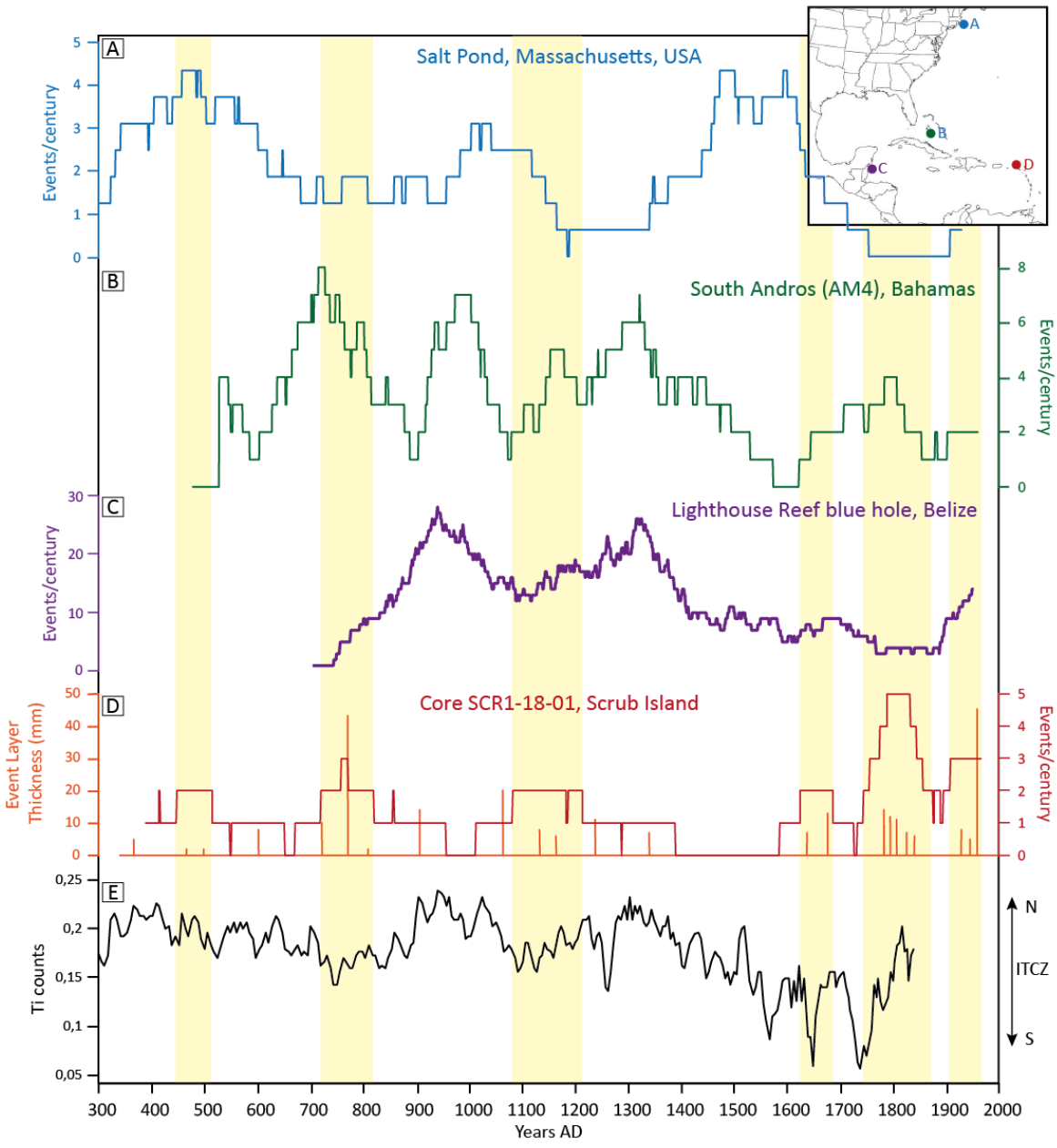

Figure 9. 101-year moving window event frequency on (A) Salt Pond, MA (Donnelly et al., 2015) (blue), (B) South Andros Island (green), (C) Lighthouse Reef Blue Hole, Belize (Denommee et al., 2014) (purple) and (D) Scrub Island (red) with the hurricane events thickness (orange). The hurricane high frequency periods from Scrub Island are highlighted with the yellow intervals. (E) presents the Ti counts from Cariaco Basin associated with the ITCZ position (Haug et al., 2001). Map in the top right corner shows the location of the sites where hurricane frequency was calculated from sediment record.